

The Chemical Basis of Thiol Addition to Nitro-Conjugated Linoleic Acid, a Protective Cell-Signaling Lipid*

Lucía Turell^{‡§1}, Darío A. Vitturi^{†1}, E. Laura Coitiño[¶], Lourdes Lebrato^{‡§}, Matías N. Möller^{¶§}, Camila Sagasti[¶], Sonia R. Salvatore[†], Steven R. Woodcock[†], Beatriz Alvarez^{‡§2}, Francisco J. Schopfer^{†3}

Laboratorios de [‡]Enzimología, [¶]Química Teórica y Computacional, and [¶]Fisicoquímica Biológica, Instituto de Química Biológica, Facultad de Ciencias, and [§]Center for Free Radical and Biomedical Research, Universidad de la República, Uruguay; [†]Department of Pharmacology and Chemical Biology, University of Pittsburgh, School of Medicine, USA.

¹ LT and DAV contributed equally

² To whom correspondence may be addressed: Laboratorio de Enzimología. Facultad de Ciencias. Iguá 4225, Montevideo, Uruguay 11400. Tel.: + (598) 2 525-0749; E-mail: beatriz.alvarez@fcien.edu.uy

³ To whom correspondence may be addressed: Dept. of Pharmacology and Chemical Biology, Thomas E. Starzl Biomedical Science Tower E1340, 200 Lothrop St., University of Pittsburgh, Pittsburgh, PA 15213. Tel.: +(1) 412-648-0193; Fax: 412-648-2229; E-mail: fjs2@pitt.edu

Running title: *Nitro-Conjugated Linoleic Acid and Thiols*

Keywords: Thiol, sulfhydryl, kinetics, nitroalkene fatty acid, human serum albumin, nitro-conjugated linoleic acid, Michael addition, elimination, nitro fatty acid.

ABSTRACT

Nitroalkene fatty acids are formed *in vivo* and exert protective and anti-inflammatory effects via reversible Michael addition to thiol-containing proteins in key signaling pathways. Nitro-conjugated linoleic acid (NO₂-CLA) is preferentially formed, constitutes the most abundant nitrated fatty acid in humans and contains two carbons that could potentially react with thiols, modulating signaling actions and levels. In this work, we examined the reactions of NO₂-CLA with low molecular weight thiols (glutathione, cysteine, homocysteine, cysteinylglycine and β-mercaptoethanol) and human serum albumin (HSA). Reactions followed reversible biphasic kinetics, consistent with the presence of two electrophilic centers in NO₂-CLA located on the β- and δ-carbons with respect to the nitro group. The differential reactivity was

confirmed by computational modeling of the electronic structure. The rates (k_{on} and k_{off}) and equilibrium constants for both reactions were determined for different thiols. LC-UV-Vis and LC-MS analyses showed that the fast reaction corresponds to β-adduct formation (the kinetic product) while the slow reaction corresponds to the δ-adduct (the thermodynamic product). The pH dependencies of the rate constants, the correlations between intrinsic reactivity and thiol pK_a and the absence of deuterium solvent kinetic isotope effects suggested stepwise mechanisms with thiolate attack on NO₂-CLA as rate-controlling steps. Computational modeling supported the mechanism and revealed additional features of the transition states, anionic intermediates and final neutral products. Importantly, the detection of cysteine-δ-adducts in human urine provided evidence for the biological relevance of this reaction. Finally, HSA was found to bind NO₂-

CLA non-covalently and to form covalent adducts at Cys34, suggesting potential modes for systemic distribution. These results provide new insights into the chemical basis of NO₂-CLA signaling actions.

Nitroalkene fatty acids are endogenous adaptive signaling mediators formed *in vivo* upon addition of nitric oxide (NO[•])- or nitrite (NO₂⁻)-derived nitrogen dioxide (NO₂[•]) to unsaturated fatty acids (1-3). The presence of the electron-withdrawing nitroalkene group renders the β-carbon electron-deficient and thus susceptible to attack by nucleophiles in reversible Michael addition reactions (4). Electrophilicity of nitroalkene fatty acids is critical to the biological actions of these molecules, as demonstrated by the inhibitory effects of increased nitroalkene reductase activity (5). Nitroalkene fatty acids exhibit potent anti-inflammatory and cytoprotective properties and thus are beneficial in many models of disease including atherosclerosis, restenosis, ischemia reperfusion, renal injury, diabetes, metabolic syndrome and endotoxemia (6-13). Furthermore, endogenous formation of nitroalkene fatty acids has been associated with the cardioprotective effects of the Mediterranean diet (14,15). Notably, the potential application of soft electrophiles as pharmacological agents is underscored by the FDA approval of dimethyl fumarate for the treatment of multiple sclerosis (16,17).

Thiols (RSH)^a are excellent nucleophiles and are able to react with different electrophiles including oxidants. This property constitutes the basis of the fundamental roles of particular thiols in signaling, detoxification and antioxidant response processes. For most chemical and enzymatic reactions, thiol reactivity involves the nucleophilic attack of the ionized thiolate (RS⁻) on the electrophile. The intracellular compartment presents an elevated concentration of reduced thiols. Glutathione (GSH) is the main low molecular weight thiol in the cytosol (2-17 mM), and protein thiols represent ~70% of the total reduced intracellular pool (18-21). In contrast, plasma has much lower total thiol concentrations which, in addition, are predominantly oxidized. Low molecular weight plasma thiols include cysteine, cysteinylglycine, GSH, homocysteine

and γ-glutamylcysteine, which together constitute a total of 12-20 μM reduced thiol. The most abundant thiol in this compartment is cysteine 34 in human serum albumin (HSA) which is ~600 μM and 75% reduced (22).

From a kinetic, mechanistic and structure-reactivity relationship aspect, Michael addition and β-elimination reactions between various activated olefins and nucleophiles have received considerable attention in the literature. Depending on the nucleophilic and electrophilic partners as well as on the reaction conditions, two types of mechanisms have been proposed: concerted or stepwise, with the latter involving intermediate carbanions (23-26).

Conjugated linoleic acid (CLA) is a preferential substrate for biological nitration leading to the formation of 9- and 12-nitro-octadecadienoic acid (9- and 12-NO₂-CLA) (27). Nitroalkene derivatives of CLA are present in plasma and urine of healthy individuals with and without CLA supplementation and are generated during digestion, metabolic stress, and inflammation (1,2,27). The reaction between thiols and NO₂-CLA has implications for the modulation of not only signaling actions, but also circulating levels and bio-elimination pathways (2,6,28). Importantly, in the case of NO₂-CLA, both the β- and δ-carbons with respect to the nitro group are, in principle, electrophilic and thus susceptible to reaction with nucleophiles.

Herein we provide an experimental and computational study of the reaction of NO₂-CLA, the most abundant endogenous nitroalkene, with biological thiols. We found that two reversible products are formed, the β-adducts and the δ-adducts. The β-adducts are formed with faster kinetics but the δ-adducts are more stable. The reaction mechanisms are stepwise, with thiolate attack on the nitroalkene as the rate-controlling step. In addition, HSA is able to bind NO₂-CLA non-covalently. Our findings contribute to the understanding of the chemical basis of the signaling and pharmacological actions of nitroalkene fatty acids.

RESULTS

NO₂-CLA reacts biphasically and reversibly with low molecular weight thiols. Stopped-flow mixing of a solution consisting of 9- and 12-NO₂-

CLA (Fig. 1A) with excess GSH led to a reduction in absorbance at 330 nm, consistent with loss of double bond conjugation. The decrease was biexponential and comprised a fast phase that lasted ~0.5 min followed by a second phase that was slower by a factor of ~30 (Fig. 1B). No significant changes in absorbance occurred in the absence of thiols. Although the NO₂-CLA stock contains an approximately 1:1 mixture of the positional isomers 9- and 12-NO₂-CLA, the existence of two phases could not be explained by a differential reactivity of the isomers, as purified 9- and 12-NO₂-CLA yielded comparable biphasic kinetics (Fig. 1B, inset). In contrast, the reaction with the monounsaturated derivative nitrooleic acid (NO₂-OA), that has only one electrophilic site, was monophasic (Fig. 1C) (29). When NO₂-CLA was mixed with the yellow thiol thionitrobenzoate (TNB), which allows to follow changes in thiol concentration instead of NO₂-CLA concentration because of its absorbance at 412 nm, the decrease in TNB absorbance was also biphasic, confirming that thiol consumption occurred in both phases (Fig. 1D). Regarding the concentration dependence of the reaction between NO₂-CLA and excess GSH, a linear dependence with a non-zero y-axis intercept was observed between the pseudo-first order rate constant (k_{obs}) of the fast phase and GSH concentration (Fig. 1E), while a hyperbolic dependence with a non-zero intercept was observed for the slow phase (Fig. 1F).

Taken together, the kinetic results are consistent with two parallel and reversible processes involving two non-equivalent electrophilic centers in NO₂-CLA. These centers react with thiols forming two products that we hypothesize are the β - and the δ -adducts according to Scheme 1, where $k_{\text{on}\beta}$ and $k_{\text{on}\delta}$ are second-order rate constants at pH 7.4 for the forward addition reaction of the fast and slow processes, respectively, and $k_{\text{off}\beta}$ and $k_{\text{off}\delta}$ correspond to first-order rate constants for the reverse elimination reactions^b.

The coupled differential equations derived from Scheme 1 can be solved in matrix form yielding complex biexponential concentration functions. The relation of the exponential constants k_{obs} with the rate constants and concentrations is simplified when one phase is faster than the other (30,31). In this case, the larger

exponential constant, $k_{\text{obs}(\text{fast})}$, increases linearly with thiol concentration according to Eq. 1 (Fig. 1E).

$$k_{\text{obs}(\text{fast})} = k_{\text{on}\beta} [\text{thiol}] + k_{\text{off}\beta} \quad \text{Eq. 1}$$

For GSH reactions, $k_{\text{on}\beta} = 34 \pm 4 \text{ M}^{-1} \text{ s}^{-1}$ was determined from the slope of the plot, while $k_{\text{off}\beta} = 0.10 \pm 0.02 \text{ s}^{-1}$ was obtained from the y-axis intercept. The equilibrium dissociation constant ($K_{\text{eq}\beta}$) was calculated by dividing $k_{\text{off}\beta}$ by $k_{\text{on}\beta}$ and its value was $(2.8 \pm 0.9) \times 10^{-3} \text{ M}$ (25 °C, pH 7.4).

The smaller exponential constant, $k_{\text{obs}(\text{slow})}$, is given by the sum of the forward and reverse effective rate constants, where the former is $k_{\text{on}\delta} [\text{thiol}]$ multiplied by the fraction of free NO₂-CLA, and increases hyperbolically with thiol concentration according to Eq. 2 (Fig. 1F).

$$k_{\text{obs}(\text{slow})} = \frac{k_{\text{on}\delta} K_{\text{eq}\beta} [\text{thiol}]}{K_{\text{eq}\beta} + [\text{thiol}]} + k_{\text{off}\delta} \quad \text{Eq. 2}$$

From fits to this equation, the $k_{\text{on}\delta}$ for the reaction with GSH was determined to be $3.5 \pm 0.5 \text{ M}^{-1} \text{ s}^{-1}$ while $K_{\text{eq}\beta}$ was $(3.0 \pm 0.2) \times 10^{-3} \text{ M}$, in excellent agreement with the value determined from the fast phase. The $k_{\text{off}\delta}$ was obtained using data at relatively low thiol concentrations and was $(3 \pm 1) \times 10^{-4} \text{ s}^{-1}$. The $K_{\text{eq}\delta}$ was $(9 \pm 5) \times 10^{-5} \text{ M}$.

Similar determinations were carried out for cysteine, homocysteine, cysteinylglycine and β -mercaptoethanol (BME) and the rate and equilibrium constants are shown in Table 1. The rate constants were higher for the presumed β -adducts in all cases. The equilibrium constants were lower by factors of 20-65 for the δ -adducts, reflecting higher stability. It is worth mentioning that at higher cysteine concentrations (30 mM) a third slow phase became evident ($k_{\text{obs}} = (1.33 \pm 0.01) \times 10^{-3} \text{ s}^{-1}$) which was no further characterized. No reaction was observed with histidine ($\leq 40 \text{ mM}$), suggesting that additions of α -amino and imidazole groups were not significant, consistent with nitrogenous bases being weaker nucleophiles towards Michael acceptors than thiolates (23,26).

NO₂-CLA has two non-equivalent electrophilic carbon centers in C _{β} and C _{δ} . The electrophilic Fukui $f^+(\text{r})$ function, that measures the propensity of NO₂-CLA to gain electron density in a nucleophilic attack, is shown in Fig. 2,

mapped on a total electronic density isosurface calculated at the PCM-DFT level in aqueous solution. Two well-defined and distinct soft electrophilic regions (depicted in blue) involving the C_β and C_δ centers are found in both isomers. Whereas the region around C_β appears extended over the molecular surface and connected to the electrophilic nitro group envelope, the region enclosing C_δ is considerably smaller. These features would make C_β more prone to nucleophilic attack by thiols. Atomic softness data calculated from global softness and condensed Fukui f_A^+ (Table 2) completes the picture enabling a quantitative comparison, showing that C_β is significantly softer than C_δ , establishing the non-equivalency of the electrophilic C_β and C_δ centers and contributing to consolidate the hypothesis of their association with the fast and slow reactions, respectively.

The β -adduct is the kinetic product and the δ -adduct the thermodynamic product. In order to define the products generated in each phase of the reaction, spectrophotometric, LC-UV-Vis and LC-MS/MS experiments were performed. First, the time course of the reaction with GSH was followed at three different wavelengths. During the fast phase the decrease in absorbance at 330 nm correlated with an increase at 250 nm, while no changes were observed at 290 nm. In the slow phase however, the decrease at 330 nm correlated with an increase at 290 nm (Fig. 3A). These results suggest that the product formed during the slow reaction contains an intact nitroalkene moiety due to thiol addition at the δ -carbon (29,32) while that formed during the fast reaction does not.

LC-UV-Vis analyses were performed using BME as a model thiol due to its slower addition kinetics and better chromatographic separation (33,34). 9-NO₂-CLA eluted at a retention time of 15.5 min (peak 1, λ_{\max} 320 nm) (Fig. 3B and C). The peak at 15.1 min (peak 1*) corresponds to contaminant 12-NO₂-CLA (data not shown). In the first 10 s of the reaction with BME a peak appeared at 8.8 min (peak 2, λ_{\max} 240 nm) (Fig. 3B, inset and Fig. 3C), that was still present after 5 min but disappeared after 1 h due to the reverse elimination process and further reactions of NO₂-CLA, and was thus assigned to the fast reaction product (β -addition). After 5 min of reaction another peak appeared at 8.2 min (peak 3, λ_{\max} 280 nm) (Fig. 3B), became dominant as the reaction

progressed, and was identified as the δ -addition product. This peak was not symmetric, suggesting the presence of two diastereomers, both with maximum absorbances at 280 nm (Fig. 3C). The secondary peaks at 8.6 (peak 2*) and 7.7 min (peak 3*) were assigned to the products of the fast and slow processes for the reaction between contaminant 12-NO₂-CLA and BME.

To obtain further mechanistic insight, the reaction between purified 9-NO₂-CLA and BME was monitored by LC-MS/MS. Figures 4A and 4B show that 9-NO₂-CLA consumption (MRM 324/46, RT 8.6 min) leads to the formation of an early addition product (MRM 402/324, RT 6.9 min, β -adduct) which decays and becomes undetectable at 60 min. The disappearance of this product coincides with the formation of two isobaric species (MRM 402/324, RT 6.5 and 6.8 min, δ_1 and δ_2 -adducts respectively) that become the dominant products during the slow phase of the reaction and likely represent diastereomers as further discussed later (Figs. 6C and 7B). To confirm the relative rates of elimination from the adducts formed during the different phases of the reaction, aliquots were incubated with excess NEM (100 mM, 30 min), to efficiently trap BME ($k = 7 \times 10^4 \text{ M}^{-1} \text{ s}^{-1}$ at pH 7.4 (35)) (Fig. 4C and D). Consistent with the measured $k_{\text{off}\beta}$ and $k_{\text{off}\delta}$ values (Table 1), NEM incubation completely reversed adducts formed at early time points but had no effect on the late products. Similar results were obtained with the purified 12-NO₂-CLA isomer, with the particularity that only one δ -addition product could be resolved to such an extent as to allow reliable peak integration (Fig. S1).

Overall, LC-MS/MS results and UV-Vis analysis were in excellent agreement and it was concluded that the fast reaction corresponded to the β -addition of the thiol and the slow reaction to the δ -addition (Scheme 1). No evidence for the formation of other products was obtained. The results are consistent with a fast reaction of NO₂-CLA with the thiol to form initially the β -adduct. Due to the reversibility of this reaction, the β -adduct undergoes elimination and releases free NO₂-CLA, which engages in further reactions finally leading to the slow accumulation of the more stable δ -adducts.

Addition requires a thiolate and elimination occurs through two independent pathways. The

pH dependence of the reaction kinetics of NO₂-CLA with GSH was studied using three-component buffers of constant ionic strength. Plots of k_{obs} versus GSH concentration were constructed at each pH, from which the corresponding apparent $k_{\text{on,app}}$ and $k_{\text{off,app}}$ values were obtained for both fast and slow processes. For the fast reaction, the $k_{\text{on}\beta,\text{app}}$ increased with pH (Fig. 5A) according to a single-p K_a equation (Eq. 3), where $k_{\text{on,pH-indep}}$ represents the rate constant for the completely ionized thiolate. The p K_a was 8.78 ± 0.02 , in agreement with the reported p K_a of GSH (8.94 (36)) and consistent with the requirement for rapid prior ionization of the thiol to thiolate in the forward addition process.

$$k_{\text{on,app}} = k_{\text{on,pH-indep}} \frac{K_a}{K_a + [\text{H}^+]} \quad \text{Eq. 3}$$

The $k_{\text{off}\beta,\text{app}}$ presented an upward bend indicative that the elimination process occurs through two independent pathways (Fig. 5B) (37). At biologically-relevant pH values, elimination appears to be unimolecular or water-assisted. The increase above pH 9 likely reflects the assistance of alternative bases. Similar pH dependencies were observed for the slow phase (data not shown), suggesting that comparable mechanisms are operative.

Correlations with thiol p K_a suggest that the thiolate participates in the rate-controlling step. Since the thiolate is the reactant in the forward addition process, the $k_{\text{on,app}}$ at pH 7.4 (Table 1) were corrected according to Eq. 3 to obtain pH-independent values ($k_{\text{on,pH-indep}}$), that reflect the intrinsic reactivity of each thiolate. For the fast reaction, the log of $k_{\text{on,pH-indep}}$ increased with thiol p K_a according to Eq. 4, where β_{nuc} is the Brønsted nucleophilic coefficient and C_{on} is a constant. According to the slope and the y-intercept of the plot, β_{nuc} was 0.64 ± 0.08 and C_{on} was -2.8 ± 0.7 (Fig. 5C, top trace).

$$\log k_{\text{on,pH-indep}} = \beta_{\text{nuc}} \text{p}K_a + C_{\text{on}} \quad \text{Eq. 4}$$

The β_{nuc} value of 0.64 indicates that thiolate nucleophilicity correlates with proton basicity and is consistent with thiolate participation in transition state formation. It also suggests a relatively high degree of charge transfer at the transition state level. For comparison, β_{nuc} values

of 0.45 and 0.16 were reported for the addition of thiols to acrylonitrile (26) and α -nitrostilbene, respectively (23).

For the reverse reaction (pH < 9), inverse correlations between the log k_{off} and thiol p K_a were obtained, consistent with Eq. 5, where β_{lg} is the Brønsted leaving group coefficient and C_{off} is a constant. The values of β_{lg} and C_{off} were determined from the slope and y-intercept of the plot to be -0.73 ± 0.12 and 5.3 ± 1.1 , respectively (Fig. 5C, bottom trace).

$$\log k_{\text{off}} = \beta_{\text{lg}} \text{p}K_a + C_{\text{off}} \quad \text{Eq. 5}$$

The β_{lg} value of -0.73 indicates that the reactivity of the adduct correlates with the proton acidity of the thiol that is eliminated. This is consistent with a rate-controlling step that involves thiolate departure and partial charge formation, with considerable amount of C-S bond breaking in the transition state, in agreement with a reversal of the mechanism proposed for the forward reaction. Values of β_{lg} of -0.68 and -0.54 were reported for the elimination of thiols from α -nitrostilbene and acrylonitrile adducts respectively, with leaving group expulsion argued to be the rate-controlling step in the latter case (23,25).

For the slow reaction, similar trends were observed, with $\beta_{\text{nuc}} = 0.6 \pm 0.2$, $C_{\text{on}} = -4 \pm 2$, $\beta_{\text{lg}} = -0.72 \pm 0.09$ and $C_{\text{off}} = 2.7 \pm 0.8$ (Fig. 5D).

Lack of solvent kinetic isotope effects. The reaction of 20 μM NO₂-CLA with 4 mM GSH exhibited k_{obs} of 0.23 ± 0.03 and $(6.4 \pm 0.2) \times 10^{-3} \text{ s}^{-1}$ for the fast and slow processes, respectively. When H₂O was replaced by D₂O (92 %) and the pD adjusted for similar GSH ionization fractions, k_{obs} were 0.25 ± 0.04 and $(6.1 \pm 0.3) \times 10^{-3} \text{ s}^{-1}$, indicating the absence of significant deuterium solvent kinetic isotope effects. This rules out rate-controlling steps that involve protonation and suggests that concerted addition-elimination processes are not involved. Instead, the reactions likely occur through stepwise mechanisms involving anionic intermediates and thiolate attack as the rate-limiting step, in agreement with the Brønsted correlations shown in Fig. 5C and 5D.

Main features of the transition states and anionic intermediates for thiolate addition on C β /C δ centers. In line with the experimental results, PCM-DFT modeling provided a detailed characterization of the transition states (TS β /TS δ)

and anionic intermediates (I_β/I_δ) for a stepwise attack by a thiolate on C_β/C_δ electrophilic centers embedded at the common central moiety of both NO_2 -CLA isomers (Fig. 6, structural data in Table S1). No evidence was found here for a concerted four-membered ring TS as reported for the attack of thiols on α,β -unsaturated carbonyls (38). Both $\text{TS}_\beta/\text{TS}_\delta$ resemble the open structures found for thio-Michael addition on that kind of acceptors (39,40), taking place after fast deprotonation of the thiolate in solution.

Reactions at C_β and C_δ proceed both through entropically disfavored loose reactant complexes ($\text{RC}_\beta/\text{RC}_\delta$, Fig. 6A and 6B) leading to transition states ($\text{TS}_\beta/\text{TS}_\delta$) with a more asymmetric distribution of charge in the acceptor and associated free-energy barriers of respectively 18.9 and 20.2 kcal/mol calculated respect to the isolated reactants in solution (Table 3). This supports the assignment of β -/ δ -addition processes respectively to the fast/slow phases observed in the experiments. In fact, a difference of 1.3 kcal/mol in activation free-energy translates into a 9-fold increase in the k_{on} rate for β -addition with respect to δ -addition, in excellent agreement with the kinetic experiments (Table 1). Charge transfer of 0.33 and 0.28 atomic units (au) between reacting moieties is respectively found at TS_β and TS_δ (mainly accommodated at the NO_2 group) reflecting the similarity between β_{nuc} parameters for both fast and slow NO_2 -CLA reactions. The R1/R2 substituents at the conjugated nitroalkene moiety (Scheme 1) modulate its intrinsic reactivity towards thiolate attack (23,26). In particular, for nitroalkene fatty acids the alkyl/carboxyl(ate) chains are expected to increase the reactivity towards thio-Michael addition with respect to the model system here studied, without altering the mechanism (Coitiño *et al.*, unpublished) leading to a more pronounced charge reorganization between partners at the C_β/C_δ addition TSs, closer to the expectations from the β_{nuc} values derived from experimental data. A similar rationale applies to bond forming/breaking at each TS, for which Wiberg bond indices (WBIs) of 0.27/0.15 for the nascent $\text{S}\cdots\text{C}_\beta/\text{S}\cdots\text{C}_\delta$ bonds imply advances of 28 % or 16 % at each reaction involving the model compounds. A lag in $\text{S}-\text{C}_\delta$ bond formation with respect to the advance in charge transfer from thiolate to nitroalkene moieties (not found in TS_β)

may explain the higher barrier found for the slower reaction leading to the δ -adduct (41).

Concerning the anionic intermediates (I_β/I_δ , Fig. 6) they both would be nitronate species, sharing a strengthened $\text{C}_\alpha\text{-N}$ bond (WBIs: 1.48 au and 1.32 au, respectively) and a net charge of -1 au localized at the NO_2 moiety in their structures. Whereas the second NO_2 -CLA unsaturation remains intact at $\text{C}_\gamma=\text{C}_\delta$ in I_β , it appears shifted into $\text{C}_\gamma=\text{C}_\beta$, in I_δ enabling a more extended electron delocalization that translates in a more stable δ -intermediate (Table 3). No evidence of formation of any stable carbanion was found. The NO_2 group progressively captures all the electronic density transferred between reactants up to completion of each of these two parallel addition processes, resulting in completely formed $\text{C}-\text{S}$ single bonds (1.85-1.86 Å, WBIs: 0.94 au) and loss of planarity at C_β/C_δ . Thus, whereas a thermodynamically disfavored nitronate I_β is obtained through a faster and slightly endoergic (but exothermic) process, the more stable I_δ would be the prevalent outcome of the addition step in the longer timescales. Reverse free-energy reaction barriers in the range of 15-22 kcal/mol (Table 3) are indicative of reversible processes leading in both cases to elimination of a thiolate, more facilitated from the β -intermediate (once again a result qualitatively in line with the relationship between k_{off} values obtained for the fast/slow processes).

As required step in reaching neutral products for these processes, protonation of the anionic intermediates has to be placed in the mechanistic scheme. Natural Population Analysis (NPA) atomic charges at $\text{C}_\alpha/\text{C}_\gamma/\text{O}$, the corresponding proton affinities ($\text{PA}_{\text{C}_\alpha}$, $\text{PA}_{\text{C}_\gamma}$ and PA_{O}) and the molecular electrostatic potential (MEP) mapped on the molecular surface are shown in Fig. 6C as the properties of I_β/I_δ nitronates that determine the kinetics and thermodynamics of proton capture in aqueous solution. Two possibilities arise here (Fig. 7): *O-protonation* leading to an aci-Nitro $\text{R}'\text{CH}=\text{NO}_2\text{H}$ derivative (aci-Nitro β -/ δ -adducts) and *$\text{C}_{\alpha/\gamma}$ -protonation* leading to nitroalkane/nitroalkene products (tautomers of the former). A protonation preference for the O-site over the C_α -site has been shown for phenylnitromethanes both by experiments under acidic and neutral conditions in aqueous solution and methanol (42-44) and by computational modeling at the B3LYP/6-31+G(d,p) level in gas-

phase (42) or mimicking aqueous solution by including two water molecules in the system (45). The latter study also presented a water-assisted mechanism for conversion of aci-Nitro species towards a nitroalkane C_α tautomer, more stable by 8.3 kcal/mol (45). PCM(IEF)- ω B97X-D/6-31+G(d,p) modeling in aqueous solution conducted here on the protonation of I_β and I_δ showed both species to be more prone for O-protonation (aci-Nitro would be thus a kinetic outcome of protonation) but all the C-protonated tautomers resulted to be more stable by 5-6 kcal/mol than their aci-Nitro counterparts. Among the final species derived from I_δ , a small 0.7 kcal/mol difference in stability would favor a C_γ -protonated nitroalkene over a C_α -protonated and unsaturated nitroalkane, being the former the most stable product achievable by all means.

Regarding stereoisomerism, while protonation at C_α must be anti-periplanar to the C_β -S bond linking the thiolate moiety that blocks any syn approach to I_β (only (R,S) or (S,R) enantiomers can be obtained among β -adducts) both syn/anti protonation appears feasible at the more accessible C_α position in I_δ (Fig. 6) yielding either (R,R), (R,S), (S,R) or (S,S) stereoisomers, an outcome that makes it possible to find enantiomers and diastereomers among the final δ -adducts.

Thus, on the basis of our calculations, a faster O-protonation of I_β/I_δ that would be followed by water-assisted tautomerization into the corresponding more stable counterparts complete the mechanism of reaction leading to the final products. According to modeling the expected products would be then a β -thio-Michael unsaturated adduct in nitroalkane form (Fig. 7A) in the short timescale and a mix of δ -thio-Michael adducts including a prevalent nitroalkene form and two companion diastereomeric unsaturated nitroalkane species (Fig 7B) in the long timescale.

NO₂-CLA-cysteine δ -addition products are found in human urine. Based on experimental and modeling results, endogenous Cys-NO₂-CLA in human urine is expected to be primarily represented by the more stable δ -addition products. Isotopically labelled Cys-9-NO₂-CLA and Cys-12-NO₂-CLA enriched in δ -adducts were synthesized, mixed in a 1:1 ratio and compared with urinary Cys-NO₂-CLA (Fig. 8). LC-MS/MS analysis is consistent with a predominant presence of the Cys- δ -adducts of 9- and 12-NO₂-CLA

versus the corresponding β -products, which presented a different chromatographic profile (Fig. S2).

NO₂-CLA reactions with HSA. Cys34 in HSA is the most abundant reduced thiol in plasma and is therefore a potential target for reaction with NO₂-CLA. In addition, HSA has a central role in fatty acid binding and transport, therefore both covalent and non-covalent interaction with NO₂-CLA might occur. The absorbance of NO₂-CLA changes with solvent polarity (λ_{\max} 330 nm in aqueous solution *versus* 312 nm in methanol), and thus it is expected to also change upon interaction with the hydrophobic binding sites in HSA. NO₂-CLA incubation with delipidated, thiol-blocked HSA resulted in a blue shift in absorbance (Fig. 9A). Titrations performed by adding aliquots of delipidated thiol-blocked HSA to a fixed amount of NO₂-CLA allowed to estimate up to 3.8 ± 0.5 NO₂-CLA bound per delipidated, thiol-blocked HSA (Fig. 9B). When titrations were carried out using lipidated (stearic acid:HSA, 5:1) thiol-blocked HSA, a similar value of 3.2 ± 0.2 NO₂-CLA per HSA was obtained indicating that NO₂-CLA was able to displace stearic acid (not shown). Fitting of the titration data to hyperbolic equations yielded global apparent dissociation constants of $(0.9 \pm 0.3) \times 10^{-6}$ M and $(1.2 \pm 0.3) \times 10^{-6}$ M for delipidated and lipidated HSA respectively, consistent with reported values for non-nitroalkene fatty acids (46).

The reactivity of Cys34 toward NO₂-CLA could not be evaluated following changes in absorbance at 330 nm because of interference from non-covalent binding. Therefore, the decay in HSA thiol concentration after incubation of reduced and lipidated HSA (50 μ M) with NO₂-CLA (300 μ M) for 1 h was assessed using 4,4'-dithiodipyridine (DTDP). SH/HSA ratios of 0.47 and 0.25 were obtained in the absence and presence of NO₂-CLA, respectively. Considering the concentrations used and the incubation time, a lower limit of $0.5 \text{ M}^{-1} \text{ s}^{-1}$ (25 °C, pH 7.4) was estimated for the rate constant.

DISCUSSION

NO₂-CLA reacts reversibly with thiols forming Michael adducts. In agreement with the presence of two electrophilic centers in NO₂-CLA, two products were detected: the β -adducts and the δ -

adducts. The β -adducts are formed with faster rates and are thus the kinetic products. In contrast, the δ -adducts are formed with slower kinetics but present higher stability, and are thus the thermodynamic products. In the case of GSH, the δ -adduct is 30 times more stable than the β -adduct.

From a mechanistic viewpoint, our experimental and computational results are consistent with a stepwise addition process where the rate-controlling step involves the nucleophilic attack of the thiolate on $\text{NO}_2\text{-CLA}$ to form an anionic intermediate, followed by proton incorporation; the reverse process would be involved in elimination. Although nitroalkanes possess relatively high carbon acidity ($\text{p}K_a$ 10.28 for nitromethane (43,47)), deprotonation rates can be outstandingly slow, with rate constants for proton transfer from nitromethane to OH^- measured at $27.6 \text{ M}^{-1} \text{ s}^{-1}$ (43,47). In fact, deprotonation has been proposed to control the rate of elimination of other activated alkanes (25). However, in the case of the reaction between $\text{NO}_2\text{-CLA}$ and thiols, the Brønsted correlations obtained together with the lack of a solvent deuterium kinetic isotopic effect rule out protonation as the rate-controlling step in the addition process (or deprotonation in the elimination).

The results obtained in this study can be generalized to predict the stability of $\text{NO}_2\text{-CLA}$ adducts as a function of thiol $\text{p}K_a$. If specific aspects of protein thiol reactivity and steric constraints are dismissed, the K_{eq} at a certain pH can be calculated from dividing k_{off} and k_{on} and combining Eqs. 3-5 to obtain Eq. 6.

$$\log K_{\text{eq}} = (\beta_{\text{lg}} - \beta_{\text{nuc}} + 1) \text{p}K_a + C_{\text{off}} - C_{\text{on}} + \log (K_a + [\text{H}^+])$$

Eq. 6

For both the β - and the δ -adducts, substitution in Eq. 6 with the β_{lg} , β_{nuc} , C_{off} and C_{on} values obtained from Fig. 5, allows the generalization that, at pH 7.4, the stability of the adducts increases as the $\text{p}K_a$ increases, so that adducts formed with relatively less acidic thiols (higher $\text{p}K_a$) are the more stable at neutral pH (Fig. 10).

Considering the wide variety of thiols present in the biological context and the reversibility of the reactions described herein, it is likely that $\text{NO}_2\text{-CLA}$ will exist as part of a dynamic pool

alternating between free and bound forms. Our study predicts that under intracellular conditions, $\text{NO}_2\text{-CLA}$ will quickly react with GSH and other low and high molecular weight thiols to initially form β -adducts. Due to the reversibility of these reactions, the β -adducts will undergo elimination and the free $\text{NO}_2\text{-CLA}$ will eventually give rise to the more stable δ -adducts. Thus, the transient formation of β -adducts could contribute to establish a dynamic buffer of $\text{NO}_2\text{-CLA}$. Considering the high concentrations of GSH (2-17 mM) and protein thiols inside cells (10-50 mM) (18,19), we can predict that if equilibrium is achieved > 99 % of the $\text{NO}_2\text{-CLA}$ pool will correspond to covalently bound forms (assuming similar reactivity for protein thiols and free cysteine). Furthermore, < 4 % of these products will correspond to β -adducts and > 96 % to δ -adducts, given the higher stability of the latter. In plasma, considering the lower concentrations of thiols ($\sim 450 \mu\text{M}$), it can be predicted that a significant fraction of the $\text{NO}_2\text{-CLA}$ pool will be non-covalently bound to HSA, probably impacting its transport and storage. Nevertheless, it is important to understand that the interaction of $\text{NO}_2\text{-CLA}$ with a particular protein thiol will be affected by the environment of the nucleophilic residue.

The adducts formed with GSH can be exported out of the cell through multi-drug resistance protein channels, which is a prominent pathway for nitroalkene fatty acid cell clearance. Once in the extracellular milieu, GSH- $\text{NO}_2\text{-CLA}$ adducts are processed by γ -glutamyl transpeptidases and dipeptidases/aminopeptidases. The resulting cysteine conjugates are excreted in the urine. A small portion of the cysteine conjugates can be N-acetylated intracellularly forming mercapturic acid derivatives (2, 28, 48).

The finding of adducts of $\text{NO}_2\text{-CLA}$ with cysteine in urine provides evidence for the *in vivo* reaction of $\text{NO}_2\text{-CLA}$ with thiols. Moreover, it is likely that these adducts were originated intracellularly by conjugation with GSH followed by cell export, removal of the glutamyl and glyceryl moieties and excretion. The fact that the Cys- $\text{NO}_2\text{-CLA}$ adducts found in urine correspond to δ -addition products is consistent with the higher stability of the δ - versus β -adducts of cysteine and GSH.

Overall, we have performed an in-depth study of the interactions of NO₂-CLA with biological thiols and HSA. As the beneficial health effects of nitroalkene fatty acids continue to be unraveled, our study contributes to the understanding of the chemistry that underlies the protective actions of these endogenously formed potential drug candidates.

EXPERIMENTAL AND COMPUTATIONAL PROCEDURES

General solutions. All experiments were performed in 0.1 M phosphate buffer at pH 7.4, containing 0.1 mM diethylenetriaminepentaacetic acid (DTPA) unless otherwise specified. Low molecular weight thiol solutions were prepared in nanopure water and used on the same day. Thionitrobenzoate (TNB) was synthesized as previously described (49). Thiol concentrations were determined with 5,5'-dithiobis(2-nitrobenzoate) (DTNB) before and after experiments using an absorption coefficient at 412 nm of 14150 M⁻¹ cm⁻¹ (50). Stearic acid solutions (100 mM) were freshly prepared in methanol (80 °C, with agitation). 4,4'-Dithiodipyridine (DTDP) solution (0.25 mM) was prepared in phosphate buffer, 0.1 M, pH 7.0.

Nitroalkene fatty acid and adduct solutions. 10-nitrooctadec-9-enoic acid (nitrooleic acid, NO₂-OA), 9- and 12-nitrooctadeca-9,11-dienoic acids (9- and 12-NO₂-CLA) or purified isomer solutions were synthesized as described (51,52). For kinetic experiments a 1:1 mixture of 9- and 12-NO₂-CLA or purified isomers solutions were prepared (2 mM in methanol) and kept at -80 °C until use. An absorption coefficient for NO₂-CLA at 330 nm in phosphate buffer of 6490 M⁻¹ cm⁻¹ was determined based on the previously reported absorption coefficient at 312 nm in methanol (11200 M⁻¹ cm⁻¹) (52). The extinction coefficient used for NO₂-OA was 8220 M⁻¹ cm⁻¹ at 270 nm in phosphate buffer (29). Isotopically labeled Cys- δ -adducts of 9- and 12-NO₂-CLA standards were synthesized by reacting an excess of ¹³C₃, ¹⁵N-Cys (500 μ M) with either 9- or 12-NO₂-CLA (10 μ M) for 60 min in 10 mM sodium phosphate buffer at pH 7.4, 25 °C. The reaction was stopped by 1:3 dilution in 10% formic acid, followed by addition of 7 volumes of methanol.

HSA solutions. HSA was delipidated with activated charcoal as described (53). Reduced HSA was prepared by incubation with β -mercaptoethanol (BME, 10 mM, 30 min, room temperature, with agitation) followed by gel filtration on PD-10 columns equilibrated with phosphate buffer (0.1 M, pH 7.4, 0.1 mM DTPA). Thiol-blocked HSA was prepared by incubating delipidated HSA with BME followed by addition of N-ethylmaleimide (NEM) (150 mM, 15 min, room temperature, with agitation), followed by gel filtration against phosphate buffer. Lipidated and reduced HSA was prepared by incubating delipidated HSA with 5:1 stearic acid (stearic acid:HSA) (30 min, room temperature, with agitation) followed by addition of BME and subsequent gel filtration. The HSA concentration was determined from the absorbance at 279 nm (ϵ = 0.531 (g/L)⁻¹ cm⁻¹, 66438 Da) (46). HSA thiols were measured with DTNB in sodium pyrophosphate buffer (0.1 M, pH 9, 5 min) (54).

UV-Vis assessment of nitroalkene fatty acid reactions with thiols. NO₂-CLA (10 μ M) was reacted with GSH (0.2-15 mM), cysteine (Cys, 0.5-7 mM), homocysteine (0.5-12 mM), cysteinylglycine (1.5-7 mM), BME (1-8 mM) and TNB (60-100 μ M). Changes in absorbance were followed at 330 nm (25 °C, pH 7.4). In some experiments, absorbance at 250 and 290 nm, or in the case of TNB, 412 nm, were also followed. For pH-dependence experiments, NO₂-CLA (10 μ M) was mixed with GSH (1-4 mM) using buffers of constant ionic strength and varying pH values (100 mM MES, 52 mM Tris and 52 mM ethanolamine) (55). The reaction of NO₂-OA (10 μ M) with GSH (0.2-2 mM) was followed at 285 nm. Absorbance determinations were done in a Varian Cary 50 spectrophotometer equipped with an Applied Photophysics RX2000 Rapid Kinetics accessory.

Kinetics in deuterium oxide. For comparison of the kinetics of the reaction of NO₂-CLA with GSH in D₂O (Millipore, 92 % final concentration) versus H₂O (50 mM phosphate buffer, pH 7.4), the fraction of ionized thiolate in D₂O was equaled to that in H₂O by calculating the pK_a in D₂O according to (56) and adjusting the pD. The value of pD was obtained by adding 0.4 to the measured pH.

Reactivity patterns in 9-/12-NO₂-CLA as explored by electronic structure computational modeling. Aqueous solution structures of 9-/12-

NO₂-CLA were fully optimized and verified by inspection of the Hessian eigenvalues at the PCM(IEF)- ω B97X-D/6-31+G(d,p) level (57-59), including non-electrostatic contributions to solvation as implemented in Gaussian09 rev. D.01 (60). Each solute was contained in a molecular shaped cavity constructed with Bondi's radii (61). ω B97X-D density functional was chosen based on its known superior performance in modeling thio-Michael additions (62). Energies of the highest occupied and lowest unoccupied Kohn-Sham orbitals (ϵ_{HOMO} and ϵ_{LUMO} respectively) were used to assess global softness S as the inverse of the global chemical hardness η , calculated as follows:

$$S^{-1} = \eta = \epsilon_{\text{LUMO}} - \epsilon_{\text{HOMO}} \quad (\text{Eq. 7})$$

The electrophilic Fukui function $f^+(r)$, measuring the propensity of NO₂-CLA to gain electron density in a nucleophilic attack, was also evaluated for each regioisomer within a finite difference approach (63), as shown in Eq. 8:

$$f^+(r) = \rho_{\text{N}+1}(r) - \rho_{\text{N}}(r) \quad (\text{Eq. 8})$$

where $\rho_{\text{N}}(r)$ and $\rho_{\text{N}+1}(r)$ represent the electron density at each point r around the molecule, respectively obtained for NO₂-CLA in the anionic state of reference (N) and after gaining one extra electron at the ground-state geometry (N+1) determined by *single-point* calculations at the same level of theory. Electrophilic sites were thus inspected by mapping $f^+(r)$ on a molecular surface of 0.0004 au isodensity by using Gaussview5 for generating the molecular graphics represented in Fig. 2 (64). To further assess differences among carbon electrophilic sites within each molecule, condensed Fukui function to each nucleus A (65) was also obtained by applying a Natural Bond Orbital (NBO) and deriving NPA atomic charges q_{A} from the corresponding population analysis (66) as expressed in Eq. 9:

$$f^+_{\text{A}} = q_{\text{A}}^{\text{N}+1} - q_{\text{A}}^{\text{N}} \quad (\text{Eq. 9})$$

Electrophilic atomic indices (condensed atomic softness, s^+_{A}) were finally obtained as shown in Eq. 10:

$$s^+_{\text{A}} = S \cdot f^+_{\text{A}} \quad (\text{Eq. 10})$$

Computational modeling of the detailed mechanism of thio-Michael additions at C _{β} /C _{δ} using representative model species.

Geometries of the reactants complex (RC), transition state (TS) and the anionic intermediate products (I) for the addition of methane thiolate at the C _{β} /C _{δ} positions of a representative conjugated nitro-olefin moiety (2-nitrohexa-2,4-diene) were fully optimized and verified at the same level of theory as previously applied for NO₂-CLA 9-/12-regioisomers. IRC reaction paths (67) correspondingly interconnecting them were generated with the HPC algorithm (68). Thermochemistry was calculated at 298 K and 1 atm under the usual Statistical Thermodynamics approaches (unscaled harmonic vibrational frequencies and rigid rotors) as implemented in Gaussian09 D.01 (60). NPA atomic charges (66) and Wiberg bond indices (WBIs) (69) were also extracted from the corresponding electronic structures. The structure and relative stability of the tautomeric products further obtained after protonation of the anionic intermediate outcoming from each thiolate direct addition on C _{β} /C _{δ} were also characterized at the same level of theory, assessing the corresponding proton affinities (PA) as Gibbs free-energy differences between the protonated and deprotonated form of each species. This approach has been recently validated by Taunton *et al.* in an integrated kinetic and computational characterization of thio-Michael adducts established between activated acrylonitriles and β -mercaptoethanol (70). Molecular graphics representing the 3D structure of the species characterized were prepared with Discovery Studio Visualizer 4.0 (Accelrys). Molecular electrostatic potential was mapped for both nitronate intermediates on a total electronic density surface of 0.004 au, obtaining graphical representations with Gaussview5 (Semichem Inc.) (64).

LC-MS/MS analysis of the reaction between NO₂-CLA and β -mercaptoethanol. 9- or 12-NO₂-CLA (10 μ M) were reacted with BME (1.76 mM) in phosphate buffer, pH 7.4, 25°C. Aliquots were removed at different time points and the reaction stopped by dilution into 2 volumes of either 10% formic acid or 100 mM NEM. Samples were allowed to react for 30 min, diluted in 15 volumes of methanol and subjected to LC-MS/MS analysis.

LC-MS/MS analysis of NO₂-CLA-thiol conjugates. NO₂-CLA and its conjugates were resolved by LC via reversed phase chromatography on an analytical C18 Luna column (2 x 100 mm, 5 μm particle size, Phenomenex) at a 0.65 mL/min flow rate using a water/0.1% acetic acid (solvent A) and acetonitrile/0.1% acetic acid (solvent B) solvent system. For BME-NO₂-CLA experiments, samples were loaded at 35% B for 0.3 min and then % B was increased to 90% in 9.7 min. At 10 min the column was washed using 100% B for 2 min before equilibrating at 35% B for an additional 3 min. For urinary Cys-NO₂-CLA measurements, lipid extracts were loaded at 5% B for 0.5 min, then the organic phase was increased to 35% over 3 min before being increased to 100% in 12 min. The column was washed for 3 min before re-equilibrating at 5% B for 2 min. MS analysis of BME-NO₂-CLA adducts was performed using an API Qtrap 4000 (Applied Biosystems, Framingham, MA) in the negative ion mode with the following settings: source temperature 550°C, curtain gas: 40, ionization spray voltage: -4500, GS1: 40, GS2: 40, declustering potential: -70V, entrance potential: 4V, collision energy: -17V and -35V (BME conjugates and free NO₂-CLA respectively), collision cell exit potential: -5V. Analysis of urinary lipid extracts were performed using an API 5000 (Applied Biosystems) with the following settings: source temperature 650°C, curtain gas: 50, ionization spray voltage: -4500, GS1: 55, GS2: 50, declustering potential: -70V, entrance potential: 4V, collision energy: -20V and -35V (cysteine conjugates and free NO₂-CLA respectively), collision cell exit potential: -5V.

The following transitions (m/z) were used: NO₂-CLA (324.3→46), BME-NO₂-CLA (402.3→324.3), Cys-NO₂-CLA (445.3→120), ¹³C₃¹⁵N Cys-NO₂-CLA (449.3→124).

LC-UV-Vis analysis of the reaction between NO₂-CLA and BME. High performance liquid chromatography experiments were performed in an Agilent 1260 Infinity instrument. 9-NO₂-CLA (100 μM) was mixed with BME (1.76 mM) in phosphate buffer at 25 °C. At increasing times (10 s, 5 min, 1 h) aliquots (70 μL) were mixed with 50% acetonitrile/10% formic acid (140 μL).

Samples (150 μL) were injected in a C18 column (Zorbax Eclipse Plus C18, 4.36 x 100 mm; 3.5 μm) and resolved using a linear gradient from 35% to 90% solution B in 19 min at a flow rate of 1 mL/min (solution B: acetonitrile/0.1% acetic acid, solution A: H₂O/0.1% acetic acid). The absorbance was registered using a diode array detector.

Determination of non-covalent NO₂-CLA binding to HSA. Increasing concentrations of thiol-blocked delipidated or lipidated HSA (0.2-10 μM) were mixed with NO₂-CLA (10 μM) in phosphate buffer and the UV-Vis spectra were recorded. Control procedures were performed in the absence of NO₂-CLA.

Reaction between NO₂-CLA and HSA thiol. Lipidated reduced HSA (50 μM) was mixed with NO₂-CLA (300 μM) or an equivalent volume of methanol (control) and incubated for 1 h (25 °C, pH 7.4). The samples were gel filtrated to remove excess NO₂-CLA and protein concentration was determined using both absorbance measurements at 279 nm and the bicinchoninic acid assay (71). The remaining free thiols were quantified using DTDP (215 μM). Protein was first removed via ultrafiltration. Thiopyridone concentration was determined at 324 nm ($\epsilon = 21400 \text{ M}^{-1} \text{ cm}^{-1}$) (50) in the ultrafiltrate after baseline subtraction.

Nitroalkene fatty acid extraction from human urine. Urine samples were collected from healthy human volunteers and used immediately (2) (University of Pittsburgh IRB PRO07110032). Briefly, C 18 SEPAK columns were conditioned with one column volume of 100% methanol, equilibrated with two 10% methanol volumes and 5 mL of urine were loaded. Columns were then washed with two volumes of 10% methanol, dried under vacuum, and lipids eluted with one volume of methanol. The solvent was evaporated and the samples re-suspended in 100 μL methanol for LC-MS/MS analysis.

Data processing and numerical simulations. Data were plotted and analyzed using OriginPro 8.0 (OriginLab) or Prism 6 (GraphPad). Unless specified, results are expressed as the mean ± standard error of independent experiments.

ACKNOWLEDGMENTS. We are grateful to Jenner Bonanata for technical assistance and to Andrés Abella (Universidad de la República) for help with the mathematics of the kinetic analysis.

CONFLICTS OF INTEREST. DAV, SRW and FJS acknowledge financial interest in Complexa Inc. No other competing financial interests are noted. The content is solely the responsibility of the authors and does not necessarily represent the official views of the National Institutes of Health.

AUTHOR CONTRIBUTIONS. LT¹ and DAV¹ prepared the manuscript, contributed to writing, designed, performed and analyzed experiments. LL performed experiments. ELC designed, performed and analyzed (with the assistance of CS in characterizing 12/9-NO₂-CLA local softness) computational modeling and wrote the corresponding sections of the manuscript. MNM designed and performed LC-UV/Vis experiments. SRS contributed to LC-MS/MS method development. SRW synthesized nitrated fatty acids. BA and FJS contributed to the overall concept, experimental design, data interpretation and manuscript preparation. All authors have given approval to the final version of the manuscript. ¹These authors contributed equally.

REFERENCES

1. Delmastro-Greenwood, M., Hughan, K. S., Vitturi, D. A., Salvatore, S. R., Grimes, G., Potti, G., Shiva, S., Schopfer, F. J., Gladwin, M. T., Freeman, B. A., and Gelhaus Wendell, S. (2015) Nitrite and nitrate-dependent generation of anti-inflammatory fatty acid nitroalkenes. *Free Radic. Biol. Med.* **89**, 333-341
2. Salvatore, S. R., Vitturi, D. A., Baker, P. R., Bonacci, G., Koenitzer, J. R., Woodcock, S. R., Freeman, B. A., and Schopfer, F. J. (2013) Characterization and quantification of endogenous fatty acid nitroalkene metabolites in human urine. *J. Lipid Res.* **54**, 1998-2009
3. Vitturi, D. A., Minarrieta, L., Salvatore, S. R., Postlethwait, E. M., Fazzari, M., Ferrer-Sueta, G., Lancaster, J. R., Jr., Freeman, B. A., and Schopfer, F. J. (2015) Convergence of biological nitration and nitrosation via symmetrical nitrous anhydride. *Nat. Chem. Biol.* **11**, 504-510
4. Schopfer, F. J., Cipollina, C., and Freeman, B. A. (2011) Formation and signaling actions of electrophilic lipids. *Chem. Rev.* **111**, 5997-6021
5. Vitturi, D. A., Chen, C. S., Woodcock, S. R., Salvatore, S. R., Bonacci, G., Koenitzer, J. R., Stewart, N. A., Wakabayashi, N., Kensler, T. W., Freeman, B. A., and Schopfer, F. J. (2013) Modulation of nitro-fatty acid signaling: prostaglandin reductase-1 is a nitroalkene reductase. *J. Biol. Chem.* **288**, 25626-25637
6. Delmastro-Greenwood, M., Freeman, B. A., and Wendell, S. G. (2014) Redox-dependent anti-inflammatory signaling actions of unsaturated fatty acids. *Annu. Rev. Physiol.* **76**, 79-105
7. Kelley, E. E., Baust, J., Bonacci, G., Golin-Bisello, F., Devlin, J. E., St Croix, C. M., Watkins, S. C., Gor, S., Cantu-Medellin, N., Weidert, E. R., Frisbee, J. C., Gladwin, M. T., Champion, H. C., Freeman, B. A., and Khoo, N. K. (2014) Fatty acid nitroalkenes ameliorate glucose intolerance and pulmonary hypertension in high-fat diet-induced obesity. *Cardiovasc. Res.* **101**, 352-363
8. Liu, H., Jia, Z., Soodvilai, S., Guan, G., Wang, M. H., Dong, Z., Symons, J. D., and Yang, T. (2008) Nitro-oleic acid protects the mouse kidney from ischemia and reperfusion injury. *Am. J. Physiol. Renal Physiol.* **295**, F942-949
9. Rudolph, T. K., Rudolph, V., Edreira, M. M., Cole, M. P., Bonacci, G., Schopfer, F. J., Woodcock, S. R., Franek, A., Pekarova, M., Khoo, N. K., Hasty, A. H., Baldus, S., and Freeman, B. A. (2010) Nitro-fatty acids reduce atherosclerosis in apolipoprotein E-deficient mice. *Arterioscler. Thromb. Vasc. Biol.* **30**, 938-945
10. Rudolph, V., Rudolph, T. K., Schopfer, F. J., Bonacci, G., Woodcock, S. R., Cole, M. P., Baker, P. R., Ramani, R., and Freeman, B. A. (2010) Endogenous generation and protective effects of nitro-fatty acids in a murine model of focal cardiac ischaemia and reperfusion. *Cardiovasc. Res.* **85**, 155-166

11. Schopfer, F. J., Cole, M. P., Groeger, A. L., Chen, C. S., Khoo, N. K., Woodcock, S. R., Golin-Bisello, F., Motanya, U. N., Li, Y., Zhang, J., Garcia-Barrio, M. T., Rudolph, T. K., Rudolph, V., Bonacci, G., Baker, P. R., Xu, H. E., Batthyany, C. I., Chen, Y. E., Hallis, T. M., and Freeman, B. A. (2010) Covalent peroxisome proliferator-activated receptor gamma adduction by nitro-fatty acids: selective ligand activity and anti-diabetic signaling actions. *J. Biol. Chem.* **285**, 12321-12333
12. Villacorta, L., Chang, L., Salvatore, S. R., Ichikawa, T., Zhang, J., Petrovic-Djergovic, D., Jia, L., Carlsen, H., Schopfer, F. J., Freeman, B. A., and Chen, Y. E. (2013) Electrophilic nitro-fatty acids inhibit vascular inflammation by disrupting LPS-dependent TLR4 signalling in lipid rafts. *Cardiovasc. Res.* **98**, 116-124
13. Wang, H., Liu, H., Jia, Z., Olsen, C., Litwin, S., Guan, G., and Yang, T. (2010) Nitro-oleic acid protects against endotoxin-induced endotoxemia and multiorgan injury in mice. *Am. J. Physiol. Renal Physiol.* **298**, F754-762
14. Charles, R. L., Rudyk, O., Prysyzhna, O., Kamynina, A., Yang, J., Morisseau, C., Hammock, B. D., Freeman, B. A., and Eaton, P. (2014) Protection from hypertension in mice by the Mediterranean diet is mediated by nitro fatty acid inhibition of soluble epoxide hydrolase. *Proc. Natl. Acad. Sci. U S A* **111**, 8167-8172
15. Fazzari, M., Trostchansky, A., Schopfer, F. J., Salvatore, S. R., Sanchez-Calvo, B., Vitturi, D., Valderrama, R., Barroso, J. B., Radi, R., Freeman, B. A., and Rubbo, H. (2014) Olives and olive oil are sources of electrophilic fatty acid nitroalkenes. *PLoS One* **9**, e84884
16. Fox, R. J., Miller, D. H., Phillips, J. T., Hutchinson, M., Havrdova, E., Kita, M., Yang, M., Raghupathi, K., Novas, M., Sweetser, M. T., Vigiuetta, V., Dawson, K. T., and Investigators, C. S. (2012) Placebo-controlled phase 3 study of oral BG-12 or glatiramer in multiple sclerosis. *N. Engl. J. Med.* **367**, 1087-1097
17. Gold, R., Kappos, L., Arnold, D. L., Bar-Or, A., Giovannoni, G., Selmaj, K., Tornatore, C., Sweetser, M. T., Yang, M., Sheikh, S. I., Dawson, K. T., and Investigators, D. S. (2012) Placebo-controlled phase 3 study of oral BG-12 for relapsing multiple sclerosis. *N. Engl. J. Med.* **367**, 1098-1107
18. Hansen, R. E., Roth, D., and Winther, J. R. (2009) Quantifying the global cellular thiol-disulfide status. *Proc. Natl. Acad. Sci. U S A* **106**, 422-427
19. Requejo, R., Hurd, T. R., Costa, N. J., and Murphy, M. P. (2010) Cysteine residues exposed on protein surfaces are the dominant intramitochondrial thiol and may protect against oxidative damage. *FEBS J.* **277**, 1465-1480
20. Gutscher, M., Pauleau, A. L., Marty, L., Brach, T., Wabnitz, G. H., Samstag, Y., Meyer, A. J., and Dick, T. P. (2008) Real-time imaging of the intracellular glutathione redox potential. *Nat. Methods* **5**, 553-559
21. Ostergaard, H., Tachibana, C., and Winther, J. R. (2004) Monitoring disulfide bond formation in the eukaryotic cytosol. *J. Cell. Biol.* **166**, 337-345
22. Turell, L., Radi, R., and Alvarez, B. (2013) The thiol pool in human plasma: the central contribution of albumin to redox processes. *Free Radic. Biol. Med.* **65**, 244-253
23. Bernasconi, C. F., and Killion, R. B. J. (1988) High intrinsic rate constant and large imbalances in the thiolate ion addition to substituted a-nitrostilbenes. *J. Am. Chem. Soc.* **110**, 7506-7512
24. Cann, P. F., and Stirling, C. J. M. (1974) Elimination and addition reactions. Part XXIII. Mechanisms of elimination in nitro-compounds bearing phenoxy and phenylthio leaving groups. *J. Chem. Soc., Perkin Trans. 2*, 820-823
25. Fishbein, J. C., and Jencks, W. P. (1988) Elimination reactions of b-cyano thioethers. Evidence for a carbanion intermediate and a change in rate-limiting step. *J. Am. Chem. Soc.* **110**, 5075-5086
26. Friedman, M., Cavins, J. F., and Wall, J. S. (1965) Relative nucleophilic reactivities of amino groups and mercaptide ions in addition reactions with a, b-unsaturated compounds. *J. Am. Chem. Soc.* **87**, 3672-3682
27. Bonacci, G., Baker, P. R., Salvatore, S. R., Shores, D., Khoo, N. K., Koenitzer, J. R., Vitturi, D. A., Woodcock, S. R., Golin-Bisello, F., Cole, M. P., Watkins, S., St Croix, C., Batthyany, C. I.,

- Freeman, B. A., and Schopfer, F. J. (2012) Conjugated linoleic acid is a preferential substrate for fatty acid nitration. *J. Biol. Chem.* **287**, 44071-44082
28. Alexander, R. L., Bates, D. J., Wright, M. W., King, S. B., and Morrow, C. S. (2006) Modulation of nitrated lipid signaling by multidrug resistance protein 1 (MRP1): glutathione conjugation and MRP1-mediated efflux inhibit nitrooleic acid-induced, PPAR γ -dependent transcription activation. *Biochemistry* **45**, 7889-7896
 29. Baker, L. M., Baker, P. R., Golin-Bisello, F., Schopfer, F. J., Fink, M., Woodcock, S. R., Branchaud, B. P., Radi, R., and Freeman, B. A. (2007) Nitro-fatty acid reaction with glutathione and cysteine. Kinetic analysis of thiol alkylation by a Michael addition reaction. *J. Biol. Chem.* **282**, 31085-31093
 30. Fersht, A. (1999) *Structure and mechanism in protein science: a guide to enzyme catalysis and protein folding*, W.H. Freeman, New York
 31. Fierke, C. A., and Hammes, G. G. (1995) Transient kinetic approaches to enzyme mechanisms. *Methods Enzymol.* **249**, 3-37
 32. Baker, P. R., Lin, Y., Schopfer, F. J., Woodcock, S. R., Groeger, A. L., Batthyany, C., Sweeney, S., Long, M. H., Iles, K. E., Baker, L. M., Branchaud, B. P., Chen, Y. E., and Freeman, B. A. (2005) Fatty acid transduction of nitric oxide signaling: multiple nitrated unsaturated fatty acid derivatives exist in human blood and urine and serve as endogenous peroxisome proliferator-activated receptor ligands. *J. Biol. Chem.* **280**, 42464-42475
 33. Schopfer, F. J., Batthyany, C., Baker, P. R., Bonacci, G., Cole, M. P., Rudolph, V., Groeger, A. L., Rudolph, T. K., Nadtochiy, S., Brookes, P. S., and Freeman, B. A. (2009) Detection and quantification of protein adduction by electrophilic fatty acids: mitochondrial generation of fatty acid nitroalkene derivatives. *Free Radic. Biol. Med.* **46**, 1250-1259
 34. Rudolph, V., Schopfer, F. J., Khoo, N. K., Rudolph, T. K., Cole, M. P., Woodcock, S. R., Bonacci, G., Groeger, A. L., Golin-Bisello, F., Chen, C. S., Baker, P. R., and Freeman, B. A. (2009) Nitro-fatty acid metabolome: saturation, desaturation, beta-oxidation, and protein adduction. *J. Biol. Chem.* **284**, 1461-1473
 35. Bednar, R. A. (1990) Reactivity and pH dependence of thiol conjugation to N-ethylmaleimide: detection of a conformational change in chalcone isomerase. *Biochemistry* **29**, 3684-3690
 36. Portillo-Ledesma, S., Sardi, F., Manta, B., Tourn, M. V., Clippe, A., Knoops, B., Alvarez, B., Coitino, E. L., and Ferrer-Sueta, G. (2014) Deconstructing the catalytic efficiency of peroxiredoxin-5 peroxidatic cysteine. *Biochemistry* **53**, 6113-6125
 37. Espenson, J. H. (1995) *Chemical kinetics and reaction mechanisms*, Second Edition ed., McGraw Hill, Inc.
 38. Mulliner, D., Wondrousch, D., and Schuurmann, G. (2011) Predicting Michael-acceptor reactivity and toxicity through quantum chemical transition-state calculations. *Org. Biomol. Chem.* **9**, 8400-8412
 39. Thomas, B. E., and Kollman, P. A. (1995) An ab initio molecular orbital study of the first step of the catalytic mechanism of thymidylate synthase: The Michael addition of sulfur and oxygen nucleophiles. *J. Org. Chem.* **60**, 8375-8381
 40. Krenske, E. H., Petter, R. C., Zhu, Z. D., and Houk, K. N. (2011) Transition States and Energetics of Nucleophilic Additions of Thiols to Substituted α,β -Unsaturated Ketones: Substituent Effects Involve Enone Stabilization, Product Branching, and Solvation. *J. Org. Chem.* **76**, 5074-5081
 41. Bernasconi, C. F. (1991) The Principle of Non-perfect Synchronization. in *Advances in Physical Organic Chemistry* (Bethell, D. ed.), Academic Press. pp 119-238
 42. Ando, K., Shimazu, Y., Seki, N., and Yamataka, H. (2011) Kinetic Study of Proton-Transfer Reactions of Phenylnitromethanes. Implication for the Origin of Nitroalkane Anomaly. *J. Org. Chem.* **76**, 3937-3945
 43. Bernasconi, C. F., Kliner, D. A. V., Mullin, A. S., and Ni, J. X. (1988) Kinetics of Ionization of Nitromethane and Phenylnitromethane by Amines and Carboxylate Ions in Me₂so Water Mixtures

- Evidence of Ammonium Ion Nitronate Ion Hydrogen-Bonded Complex-Formation in Me₂SO-Rich Solvent Mixtures. *J. Org. Chem.* **53**, 3342-3351
44. Moutiers, G., Thuet, V., and Terrier, F. (1997) The nitroalkane behaviour of (4-nitrophenyl)nitromethane: A kinetic and structural study in H₂O-Me₂SO mixtures. *J. Chem. Soc., Perkin Trans 2*, 1479-1486
 45. Sato, M., Kitamura, Y., Yoshimura, N., and Yamataka, H. (2009) Proton-Transfer Reactions of Nitroalkanes: The Role of aci-Nitro Species. *J. Org. Chem.* **74**, 1268-1274
 46. Peters, T. (1996) *All about albumin. Biochemistry, genetics and medical applications*, Academic Press, San Diego
 47. Bell, R. P., and Goodall, D. M. (1966) Kinetic hydrogen isotope effects in the ionization of some nitroparaffins. *Proc. R. Soc. Lond. A Math. Phys. Sci.* **294**, 273-297
 48. Ramsay, E. E., and Dilda, P. J. (2014) Glutathione S-conjugates as prodrugs to target drug-resistant tumors. *Front. Pharmacol.* **5**, 181
 49. Turell, L., Botti, H., Carballal, S., Ferrer-Sueta, G., Souza, J. M., Duran, R., Freeman, B. A., Radi, R., and Alvarez, B. (2008) Reactivity of sulfenic acid in human serum albumin. *Biochemistry* **47**, 358-367
 50. Riener, C. K., Kada, G., and Gruber, H. J. (2002) Quick measurement of protein sulfhydryls with Ellman's reagent and with 4,4'-dithiodipyridine. *Anal. Bioanal. Chem.* **373**, 266-276
 51. Woodcock, S. R., Bonacci, G., Gelhaus, S. L., and Schopfer, F. J. (2013) Nitrated fatty acids: synthesis and measurement. *Free Radic. Biol. Med.* **59**, 14-26
 52. Woodcock, S. R., Salvatore, S. R., Bonacci, G., Schopfer, F. J., and Freeman, B. A. (2014) Biomimetic nitration of conjugated linoleic acid: formation and characterization of naturally occurring conjugated nitrodienes. *J. Org. Chem.* **79**, 25-33
 53. Chen, R. F. (1967) Removal of fatty acids from serum albumin by charcoal treatment. *J. Biol. Chem.* **242**, 173-181
 54. Alvarez, B., Carballal, S., Turell, L., and Radi, R. (2010) Formation and reactions of sulfenic acid in human serum albumin. *Methods Enzymol.* **473**, 117-136
 55. Ellis, K. J., and Morrison, J. F. (1982) Buffers of constant ionic strength for studying pH-dependent processes. *Methods Enzymol.* **87**, 405-426
 56. Jencks, W. P., and Salvesen, K. (1971) Equilibrium deuterium isotope effects on the ionization of thiol acids. *J. Am. Chem. Soc.* **93**, 4433-4436
 57. Chai, J. D., and Head-Gordon, M. (2008) Long-range corrected hybrid density functionals with damped atom-atom dispersion corrections. *Phys. Chem. Chem. Phys.* **10**, 6615-6620
 58. Ditchfield, R., Hehre, W. J., and Pople, J. A. (1971) Self-Consistent Molecular-Orbital Methods. IX. An Extended Gaussian-Type Basis for Molecular-Orbital Studies of Organic Molecules. *J. Chem. Phys.* **54**, 724-728
 59. Tomasi, J. (2011) Selected features of the polarizable continuum model for the representation of solvation. *Wiley Interdisciplinary Reviews: Computational Molecular Science* **1**, 855-867
 60. Frisch, M. J., Trucks, G. W., Schlegel, H. B., Scuseria, G. E., Robb, M. A., Cheeseman, J. R., Scalmani, G., Barone, V., Mennucci, B., Petersson, G. A., Nakatsuji, H., Caricato, M., Li, X., Hratchian, H. P., Izmaylov, A. F., Bloino, J., Zheng, G., Sonnenberg, J. L., Hada, M., Ehara, M., Toyota, K., Fukuda, R., Hasegawa, J., Ishida, M., Nakajima, T., Honda, Y., Kitao, O., Nakai, H., Vreven, T., Montgomery Jr., J. A., Peralta, J. E., Ogliaro, F., Bearpark, M. J., Heyd, J., Brothers, E. N., Kudin, K. N., Staroverov, V. N., Keith, T., Kobayashi, R., Normand, J., Raghavachari, K., Rendell, A. P., Burant, J. C., Iyengar, S. S., Tomasi, J., Cossi, M., Rega, N., Millam, N. J., Klene, M., Knox, J. E., Cross, J. B., Bakken, V., Adamo, C., Jaramillo, J., Gomperts, R., Stratmann, R. E., Yazyev, O., Austin, A. J., Cammi, R., Pomelli, C., Ochterski, J. W., Martin, R. L., Morokuma, K., Zakrzewski, V. G., Voth, G. A., Salvador, P., Dannenberg, J. J., Dapprich, S., Daniels, A. D., Farkas, Ö., Foresman, J. B., Ortiz, J. V., Cioslowski, J., and Fox, D. J. (2013) Gaussian 09. Revision D.01 Ed., Gaussian, Inc., Wallingford, CT, USA
 61. Bondi, A. (1964) Van Der Waals Volumes + Radii. *J. Phys. Chem.* **68**, 441-&

62. Smith, J. M., Jami Alahmadi, Y., and Rowley, C. N. (2013) Range-Separated DFT Functionals are Necessary to Model Thio-Michael Additions. *J. Chem. Theory Comput.* **9**, 4860-4865
63. Geerlings, P., De Proft, F., and Langenaeker, W. (2003) Conceptual density functional theory. *Chem. Rev.* **103**, 1793-1873
64. Dennington, R., Keith, T., and Millam, J. (2009) GaussView Version 5. Semichem Inc, Shawnee Mission, KS.
65. Yang, W., and Mortier, W. J. (1986) The Use of Global and Local Molecular-Parameters for the Analysis of the Gas-Phase Basicity of Amines. *J. Am. Chem. Soc.* **108**, 5708-5711
66. Glendening, E. D., Landis, C. R., and Weinhold, F. (2012) Natural bond orbital methods. *Wires Comput. Mol. Sci.* **2**, 1-42
67. Fukui, K. (1981) The Path of Chemical-Reactions - the Irc Approach. *Acc Chem Res* **14**, 363-368
68. Hratchian, H. P., and Schlegel, H. B. (2005) Using Hessian updating to increase the efficiency of a Hessian based predictor-corrector reaction path following method. *J. Chem. Theory Comput.* **1**, 61-69
69. Wiberg, K. B. (1968) Application of the pople-santry-segal CNDO method to the cyclopropylcarbinyl and cyclobutyl cation and to bicyclobutane. *Tetrahedron* **24**, 1083-1096
70. Krishnan, S., Miller, R. M., Tian, B. X., Mullins, R. D., Jacobson, M. P., and Taunton, J. (2014) Design of Reversible, Cysteine-Targeted Michael Acceptors Guided by Kinetic and Computational Analysis. *J. Am. Chem. Soc.* **136**, 12624-12630
71. Smith, P. K., Krohn, R. I., Hermanson, G. T., Mallia, A. K., Gartner, F. H., Provenzano, M. D., Fujimoto, E. K., Goeke, N. M., Olson, B. J., and Klenk, D. C. (1985) Measurement of protein using bicinchoninic acid. *Anal. Biochem.* **150**, 76-85

FOOTNOTES

* This work was supported by grants and fellowships from CSIC (Universidad de la República, Uruguay) (to LT, MNM and BA), Agencia Nacional de Investigación e Innovación (ANII, Uruguay) (to LL), NIH grants K01-HL133331 (DAV), R01-AT006822 (FJS) and AHA #14GRNT20170024 (FJS). BA, ELC, LT and MNM are active members of the National System of Researchers (SNI, ANII) and of PEDECIBA (Uruguay).

^aThe abbreviations used are: RSH, thiol; GSH, reduced glutathione; BME, β -mercaptoethanol; Cys, cysteine; HSA, human serum albumin; SH/HSA, mol of thiol per mol of HSA; NO₂-CLA, nitro-conjugated linoleic acid; NO₂-OA, nitro-oleic acid; DTNB, 5,5'-dithiobis(2-nitrobenzoate); TNB, 5-thio 2-nitrobenzoate; DTDP, 4,4'-Dithiodipyridine; DTPA, diethylenetriaminepentaacetic acid; NEM, N-ethylmaleimide; MRM, multiple reaction monitoring; LC-MS/MS, liquid chromatography-tandem mass spectrometry; au, atomic units.

^b $k_{\text{on}\beta}$ and $k_{\text{on}\delta}$ are $k_{\text{on}\beta, \text{pH}7.4}$ and $k_{\text{on}\delta, \text{pH}7.4}$, the apparent rate constants at pH 7.4. The same applies to $k_{\text{off}\beta}$ and $k_{\text{off}\delta}$, but the notation was simplified for clarity.

Table 1. Apparent rate and equilibrium constants at pH 7.4 (25 °C) of the reaction of NO₂-CLA with thiols

Thiol ^a	Fast reaction (β)			Slow reaction (δ)			pK _a ^g
	$k_{onβ}$ (M ⁻¹ s ⁻¹)	$k_{offβ}$ (s ⁻¹)	$K_{eqβ}$ (M) (x10 ⁻³)	$k_{onδ}$ (M ⁻¹ s ⁻¹)	$k_{offδ}$ (s ⁻¹) (x10 ⁻⁴)	$K_{eqδ}$ (M) (x10 ⁻⁴)	
Glutathione	34 ± 4 ^d	0.10 ± 0.02 ^d	2.8 ± 0.9	3.5 ± 0.5 ^e	3 ± 1 ^c	0.9 ± 0.4	8.94
Glutathione (9-NO ₂ -CLA)	33 ± 7 ^f	0.12 ± 0.02 ^f	4 ± 1	3.5 ± 0.3 ^f	n. d. ^h	n. d. ^h	
Glutathione (12-NO ₂ -CLA)	31 ± 8 ^f	0.15 ± 0.02 ^f	5 ± 2	5.6 ± 0.6 ^f	n. d. ^h	n. d. ^h	
Glutathione (NO ₂ -OA)	64 ± 1 ^f	(6 ± 1) x 10 ⁻³ ^f	0.09 ± 0.02	Absent	Absent		
Cysteine	32.6 ± 0.2 ^b	0.196 ± 0.002 ^b	6.0 ± 0.1	2.8 ± 0.4 ^c	6 ± 3 ^c	2 ± 1	8.29
Homocysteine	18.9 ± 0.5 ^c	0.03 ± 0.02 ^c	2 ± 1	1.4 ± 0.2 ^c	1 ± 1 ^c	1 ± 1	9.10
Cysteinylglycine	51 ± 4 ^b	0.28 ± 0.06 ^b	5 ± 2	10 ± 2 ^c	10 ± 5 ^f	1.0 ± 0.7	7.95
β-Mercaptoethanol	15 ± 2 ^b	0.019 ± 0.005 ^b	1.3 ± 0.6	3.0 ± 0.4 ^c	0.6 ± 0.5 ^c	0.2 ± 0.2	9.60
Thionitrobenzoate ⁱ	~800	n. d. ^h		~50	n. d. ^h		

^a A mixture of 9- and 12-NO₂-CLA was used unless otherwise specified.

^{b, c, d, e} Values are the mean ± standard error of n = ^b2, ^c3, ^d4 or ^e5 replicates.

^f n = 1, values are the parameter ± error of the fit.

^g Thiol pK_a values reported in (36).

^h n. d., not determined.

ⁱ Because of the high absorptivity of TNB, only rough estimates of k_{on} could be obtained.

Table 2. Atomic softness s_A^+ for the carbon centers in the conjugated nitroalkene moieties embedded in each NO₂-CLA regioisomer (in au)^a

Regioisomer	Carbon center			
	C _α	C _β	C _γ	C _δ
9-NO ₂ -CLA	-0.036	<u>0.684</u>	-0.113	0.462
12-NO ₂ -CLA	-0.029	<u>0.699</u>	0.117	0.523

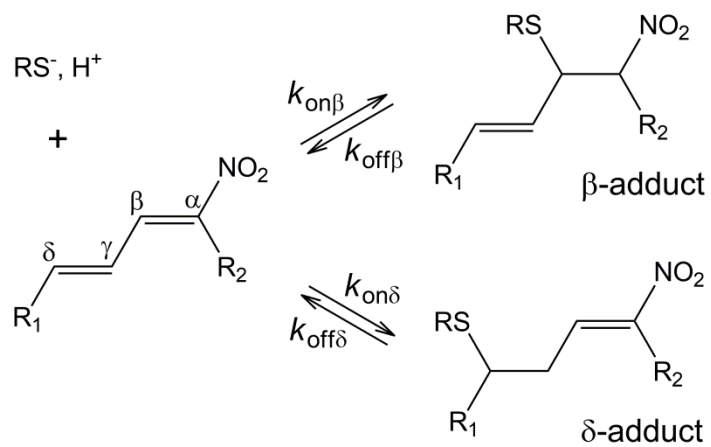
^aDetermined according to Eq. 10. Positive values correspond to atoms more prone to receive electrons, acting as electrophilic centers. The softest, most reactive C_β site in each isomer appears underlined.

Table 3. Relative energetics of the species participant in β/δ channels using a representative conjugated nitroalkene model. Enthalpy and Gibbs free-energy at 298 K and 1 atm relative to isolated reactants for each species involved in the stepwise mechanism for the thio-Michael addition and further protonation are calculated at the PCM(IEF,water)- ω B97X-D/6-31+G(d,p) level and expressed in kcal/mol.

Reaction		Thiolate addition step ^a				Protonation step - Final products ^b		
		RC _x	TS _x	I _x		Aci-Nitro (O-protonated)	Nitroalkane (C α -protonated)	Nitroalkene (C γ -protonated)
β -adduction	ΔH	2.6	6.5	-8.4	Kinetic product	-289.5	-297.3	not formed
	ΔG	12.5	18.9	3.9		-278.7	-284.9	
δ -adduction	ΔH	2.8	7.6	-14.5	Thermodynamic product	-294.8	-299.8	-300.4
	ΔG	11.6	20.2	-1.5		-283.1	-287.7	-288.4

^a X = β or δ , see the corresponding structures in Figure 6.

^b See the corresponding structures in Figure 7.



Scheme 1. Reactions between NO_2 -CLA and low molecular weight thiols. $R_1 = (CH_2)_5CH_3$ for 9- NO_2 -CLA or $(CH_2)_7CO_2H$ for 12- NO_2 -CLA, $R_2 = (CH_2)_7CO_2H$ for 9- NO_2 -CLA or $(CH_2)_5CH_3$ for 12- NO_2 -CLA, RS^- = thiolate.

FIGURE LEGENDS

SCHEME 1. Reactions between NO₂-CLA and low molecular weight thiols. R₁ = (CH₂)₅CH₃ for 9-NO₂-CLA or (CH₂)₇CO₂H for 12-NO₂-CLA, R₂ = (CH₂)₇CO₂H for 9-NO₂-CLA or (CH₂)₅CH₃ for 12-NO₂-CLA, RS⁻ = thiolate.

FIGURE 1. Reactions of NO₂-CLA with thiols at pH 7.4. (A) Structures of 9- and 12-nitro-conjugated linoleic acid (9- and 12-NO₂-CLA) and of 10-nitro-oleic acid (10-NO₂-OA) showing the electrophilic β or δ carbons. (B) A mixture of 9- and 12-NO₂-CLA (~10 μM) was mixed with GSH (3 mM) in phosphate buffer (0.1 M) containing DTPA (0.1 mM) at pH 7.4 and 25 °C, and the absorbance at 330 nm was registered. The black trace represents the best fit to a biexponential function. (Inset) Purified 9-NO₂-CLA (black trace) or 12-NO₂-CLA (gray trace) were mixed with GSH as in B. (C) NO₂-OA (10 μM) was mixed with GSH (0.6 mM) and the absorbance at 285 nm was registered. (Inset) The *k*_{obs} values at increasing GSH concentrations (0.2-2 mM) were determined from the best fit to single exponential functions. The symbols represent the mean ± standard error (n = 4). Some errors are smaller than symbols. (D) NO₂-CLA (~10 μM) was mixed with TNB (90 μM) and the absorbance at 412 nm was recorded. (E) The *k*_{obs} for the fast phase of the reaction between NO₂-CLA and GSH were determined from kinetic traces as in B. Different symbols represent the mean ± standard error of representative independent experiments; squares, n = 3; circles, n = 4. (F) Same as in E but *k*_{obs} corresponds to the slow phase; circles, n = 1; squares, mean ± standard error, n ≥ 3.

FIGURE 2. Electrophilic centers in 9-/12-NO₂-CLA regioisomers. Fukui f⁺(r) function for nucleophilic attack mapped on a total electron density surface of 0.0004 au as determined in aqueous solution at the PCM(IEF)-ωB97X-D/6-31+G(d,p) level of theory. Positive areas depicted in blue represent the electrophilic regions. The coloring scheme spans from -6.0 × 10⁻⁷ au in red to 1.1 × 10⁻⁴ au in blue.

FIGURE 3. UV-Vis analysis of the reaction between NO₂-CLA and thiols. (A) Time course changes in absorbance at 330 (open circles), 290 (black circles) and 250 nm (open triangles) for the reaction between NO₂-CLA (10 μM) and GSH (3 mM). (B) Representative LC-UV-Vis traces of the reaction between purified 9-NO₂-CLA (100 μM) and BME (1.76 mM). Aliquots were obtained at the indicated time points before LC-UV-Vis analysis. (C) UV-Vis spectra for 9-NO₂-CLA (1) and both β- (2) and δ-adducts (3). Asterisks indicate minor peaks derived from contaminant 12-NO₂-CLA.

FIGURE 4. LC-MS/MS analysis of the reaction between NO₂-CLA and BME. (A) Purified 9-NO₂-CLA (10 μM) was reacted with BME (1.76 mM) and aliquots obtained at 10 s (top), 5 min (middle) and 60 min (bottom) for analysis of free NO₂-CLA (right) and BME-NO₂-CLA adducts (left). (B) Representative time-course for 9-NO₂-CLA reaction with BME. (C-D) Aliquots collected at the indicated times were incubated with NEM (100 mM) and the percentage of free NO₂-CLA with respect to that at time zero (C) and the percentage of BME-NO₂-CLA adduct with respect to NEM-untreated controls (D) were determined. Data are representative from 3 independent experiments.

FIGURE 5. pH-dependence and correlations with thiol p*K*_a. (A-B) The fast reaction between GSH and NO₂-CLA was studied at different pHs using three-component, constant ionic strength buffers. Apparent *k*_{onβ} (A) and *k*_{offβ} (B) were obtained as in Fig. 1E and Eq. 1, from the fit of plots of *k*_{obs} versus GSH concentration to a straight line; the error bars represent the standard error of the fit. (C-D) Brønsted plots for fast (C) and slow (D) reactions. The logarithm of *k*_{on,pH-indep} rate constants (circles, calculated from *k*_{on} values at pH 7.4) and *k*_{off} (squares) were plotted against thiol p*K*_a values. Data from (Table 1); a, cysteinylglycine; b, cysteine; c, GSH; d, homocysteine; e, BME.

FIGURE 6. Structural features of the species involved in β- and δ-adduction as determined by PCM-DFT modeling in aqueous solution using CH₃S⁻ as representative thiol and a model 2-nitrohexa-2,4-diene compound containing the reactive region of NO₂-CLA. (A-B) Reactants Complex, Transition State, and

nitronate Intermediate respectively characterized for thiolate β -adduction (RC_β , TS_β and I_β) or δ -adduction (RC_δ , TS_δ and I_δ). Atoms are colored by element and a selection of relevant bond lengths, Wiberg bond order indices (WBI) and Natural Population Analysis (NPA) atomic/group charges labeled as q_X , (X representing an atom or group of atoms) featuring geometrical and electronic reorganization along each reaction channel is highlighted in proximity to the structures. Net charge transfer between reactants is evidenced at each TS. (C) Relevant properties towards I_β/I_δ nitronate protonation: molecular electrostatic potential (MEP) mapped on a total electron-density surface of 0.004 au (notice that the underlying structures retain the orientation shown immediately above in panels A and B for each species), NPA atomic charges, and proton affinities (PA) at each O/C protonation site. All properties calculated at the PCM(IEF)- ω B97X-D/6-31+G(d,p) level in aqueous solution. MEP coloring scheme spans from -0.245 (red) to -0.04 au (cyan-blue). While electrostatics favors a faster protonation at NO_2 oxygens in both cases, $C_{\omega\gamma}$ targets lead to more stable products, displaying mostly *anti* stereochemistry due to steric restrictions, as evidenced in red labels.

FIGURE 7. Structural features of the possible neutral products characterized at the PCM(IEF)- ω B97X-D/6-31+G(d,p) level in aqueous solution. (A) O-protonated aci-Nitro and C_α -protonated nitroalkane β -adducts. (B) O-protonated aci-Nitro, C_α -protonated nitroalkane and C_γ -protonated nitroalkene δ -adducts. Atoms are colored by element and a selection of the more relevant bond lengths and angles, Wiberg bond indices (WBIs) and NPA atomic charges on O, C_α and C_γ obtained at the same level of theory are reported in the proximity of relevant bonds and atoms at each structure. The expected kinetic and thermodynamic prevalent products (C_α -protonated nitroalkane β -adduct and C_γ -protonated nitroalkene δ -adduct, respectively) are framed in red.

FIGURE 8. LC-MS/MS profile of endogenous δ -Cys- NO_2 -CLA addition products in human urine. Comparison of isotopically labeled standards generated from the δ -addition of cysteine to (A) 9- NO_2 -CLA, (B) 12- NO_2 -CLA, (C) a 1:1 mixture of both standards, and (D) urine Cys- NO_2 -CLA. Data was obtained from a single urine donor with LC-MS/MS profiles consistent with published reports (1,2).

FIGURE 9. NO_2 -CLA binding to HSA. (A) UV-Vis spectra of 16 μ M thiol-blocked delipidated HSA (gray trace), 10 μ M NO_2 -CLA (black trace) and the combination of both reagents (dashed trace). (B) Thiol-blocked delipidated HSA (0.2-10 μ M) was mixed with NO_2 -CLA (10 μ M) and UV-Vis spectra were recorded. The absorbance at 310 nm was plotted against HSA concentration and the amount of NO_2 -CLA bound was determined from the change in the slope (open circles). A control without NO_2 -CLA was included (black circles).

FIGURE 10. Predicted stability of the adducts at pH 7.4 as a function of thiol pK_a . The logarithm of the apparent dissociation equilibrium constant (K_{eq}) at pH 7.4 of β - (black) and δ - (gray) adducts were calculated from Eq. 6 using parameters obtained from Fig. 5.

FIGURE 1

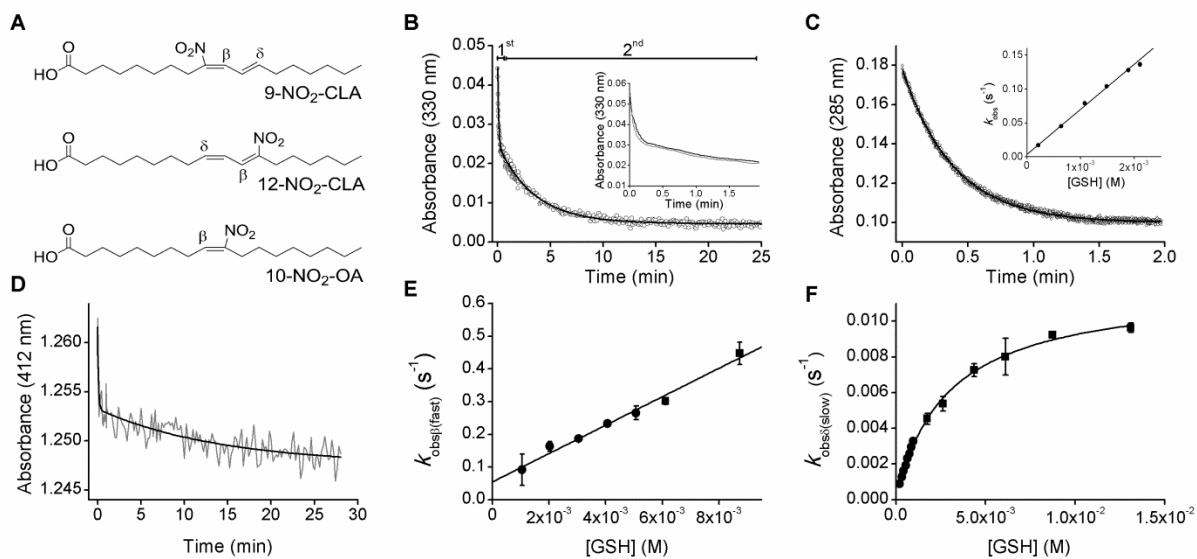


FIGURE 2

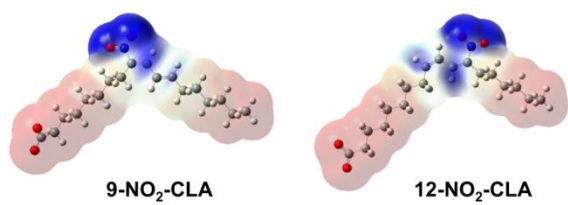


FIGURE 3

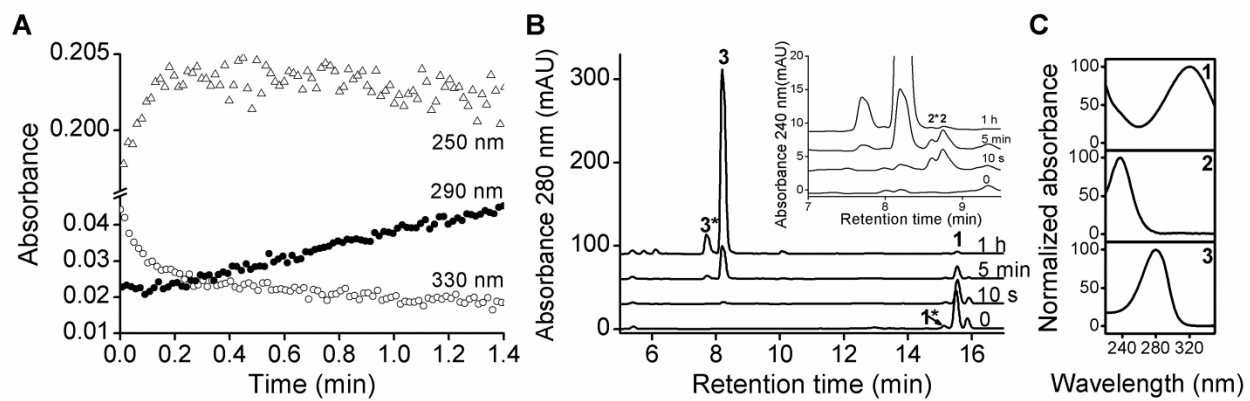


FIGURE 4

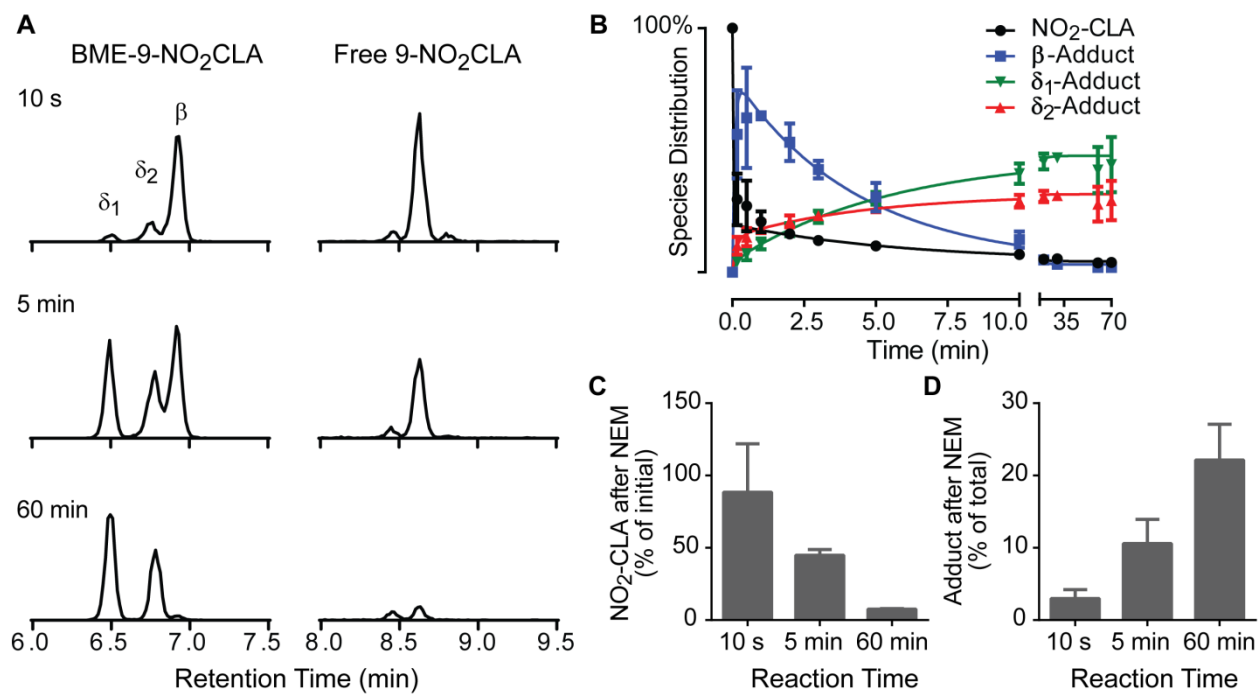


FIGURE 5

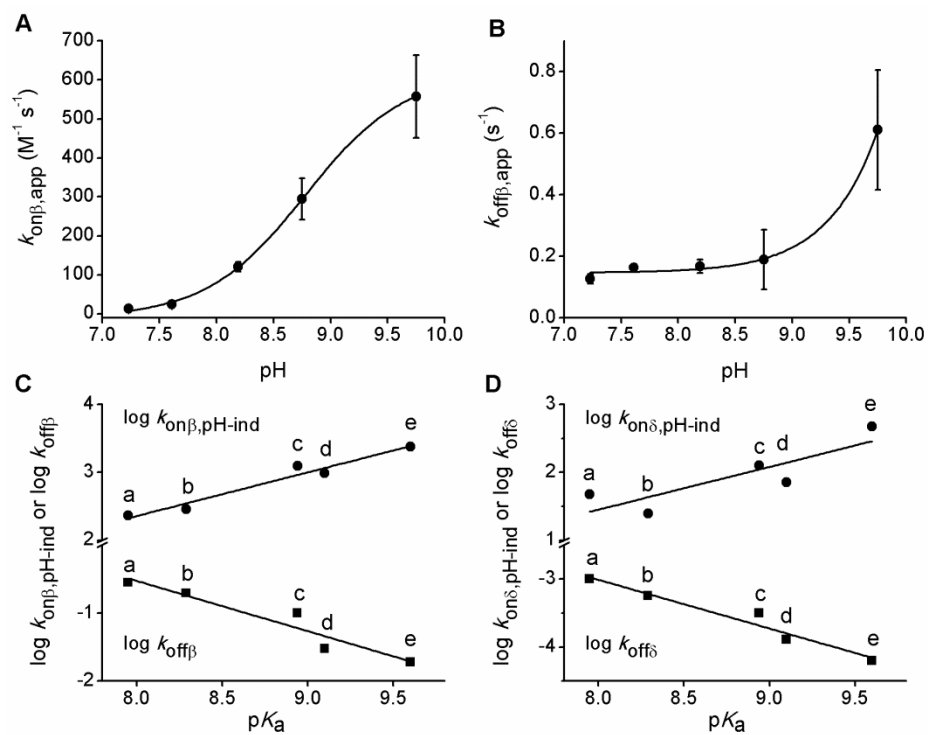


FIGURE 6

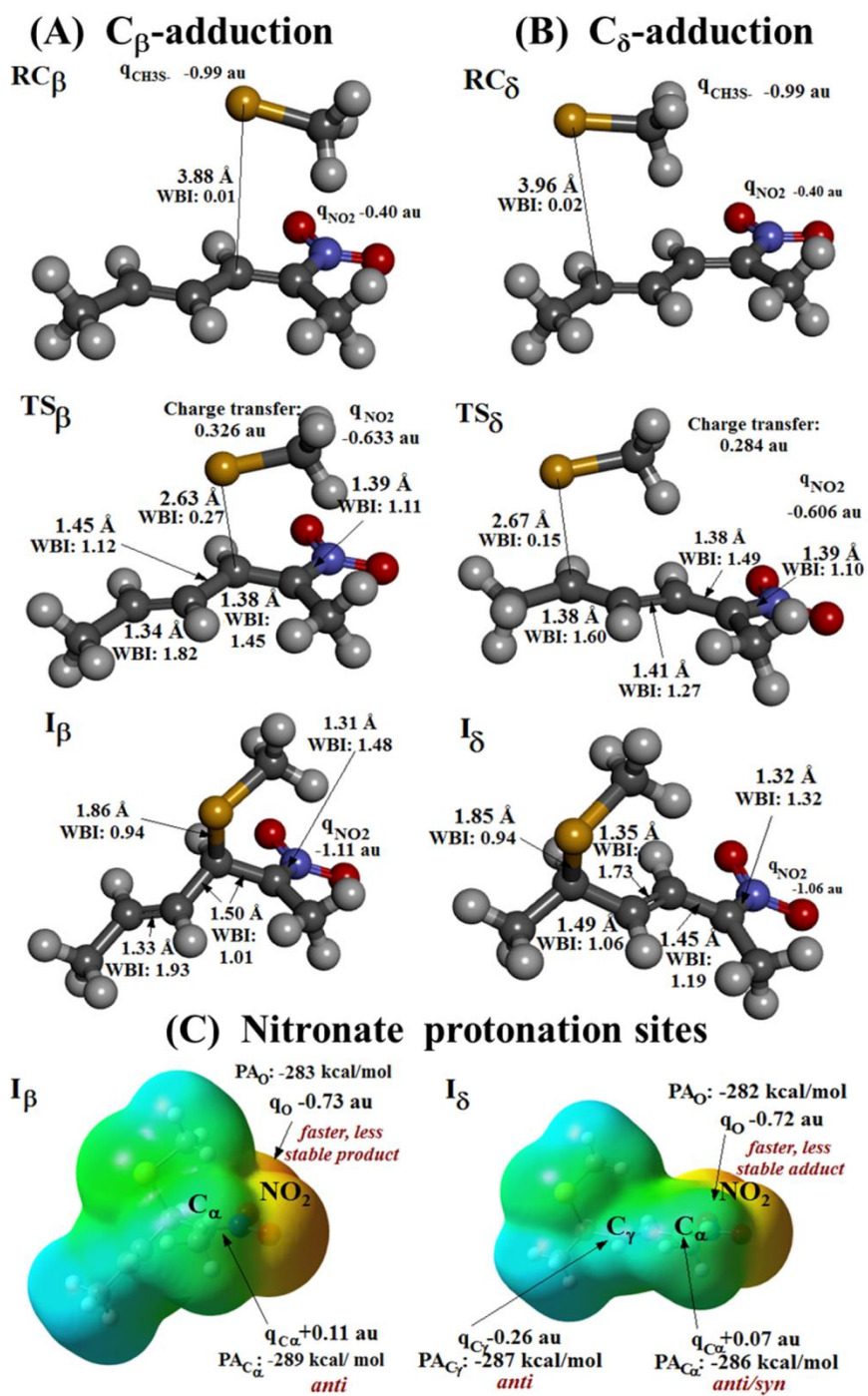


FIGURE 7

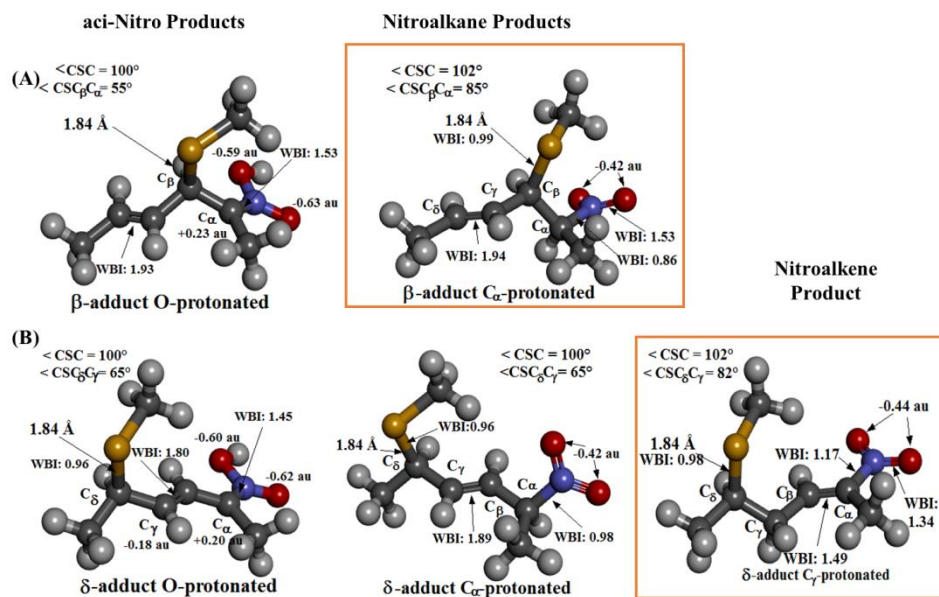


FIGURE 8

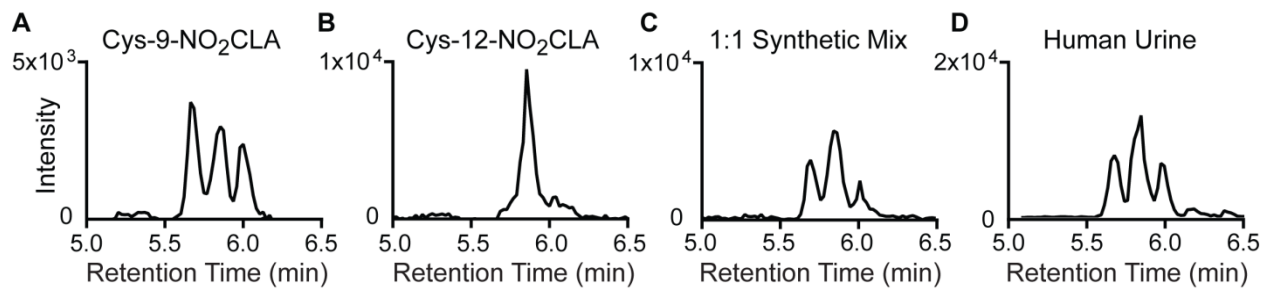


FIGURE 9

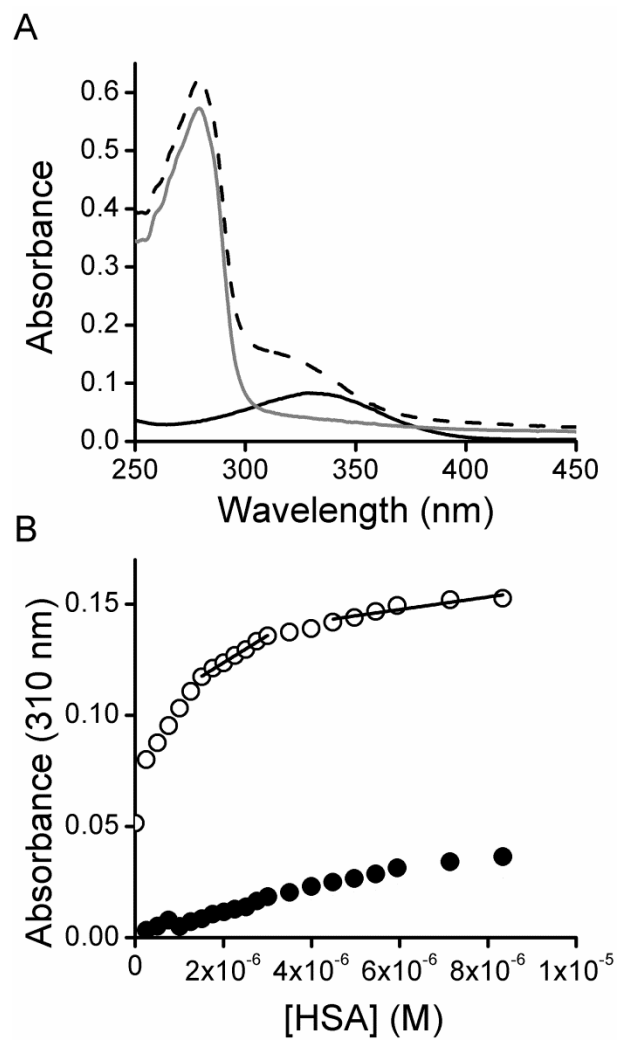
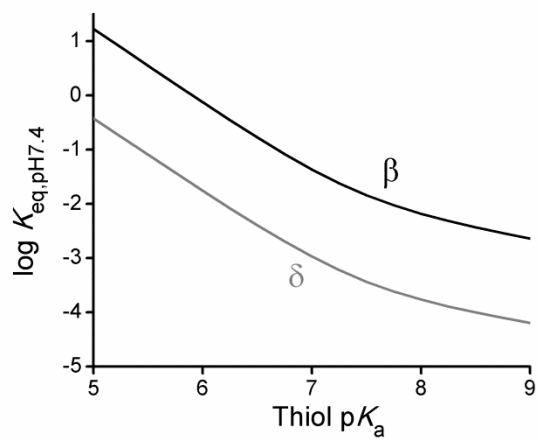


FIGURE 10



The Chemical Basis of Thiol Addition to Nitro-Conjugated Linoleic Acid, a Protective Cell-Signaling Lipid

Lucia Turell, Dario A. Vitturi, E. Laura Coitiño, Lourdes Lebrato, Matias N. Moller, Camila Sagasti, Sonia R. Salvatore, Steven R. Woodcock, Beatriz Alvarez and Francisco J. Schopfer

J. Biol. Chem. published online December 6, 2016

Access the most updated version of this article at doi: [10.1074/jbc.M116.756288](https://doi.org/10.1074/jbc.M116.756288)

Alerts:

- [When this article is cited](#)
- [When a correction for this article is posted](#)

[Click here](#) to choose from all of JBC's e-mail alerts

Supplemental material:

<http://www.jbc.org/content/suppl/2016/12/06/M116.756288.DC1>